Supplemental Material for "Disorder-induced Strongly Correlated Photons in Waveguide QED"

Guoqing Tian,[1] Li-Li Zheng,[2] Zhi-Ming Zhan,[2] Franco Nori,[3,4] and Xin-You Lü[1,*]

[1] *School of Physics and Institute for Quantum Science and Engineering, Huazhong University of Science and Technology, and Wuhan institute of quantum technology, Wuhan, 430074, P. R. China*
[2] *School of Artificial Intelligence, Jianghan University, Wuhan 430074, China*
[3] *Quantum Computing Center, RIKEN, Wakoshi, Saitama 351-0198, Japan*
[4] *Department of Physics, The University of Michigan, Ann Arbor, Michigan 48109-1040, USA*

(Dated: September 18, 2025)

* xinyoulu@hust.edu.cn

This supplemental materials contain eight parts: I. A detailed derivation of the second-order equal-time correlation function; II. Analytical calculations of the probability of photon antibunching (PA) and perfect photon blockade (PPB) for few-qubit systems; III. The physical mechanism of nearly perfect photon blockade (NPPB); IV. Correlation functions in weak- and strong-disorder limit; V. Effects of losses on non-waveguide modes; VI. Effects of chirality in coupling to waveguide modes; VII. Effects of finite bandwidth of input state; VIII. The details of numerical method used in this work.

CONTENTS

I. DERIVATION OF SECOND-ORDER CORRELATION FUNCTION

In this section, we present the Gorini-Kossakowski-Sudarshan-Lindblad master equation for our setup and, by incorporating the input-output formalism, derive the formal expressions for the correlation functions in the transmission and reflection outputs. To this end, we consider a one-dimensional array of N qubits coupled to a single optical waveguide bath. Under the rotating-wave approximation, the time evolution of the system is governed by the Hamiltonian

$$H=\sum_{m=1}^{N}\omega_m\sigma_m^\dagger\sigma_m+\sum_{\mu=\mathrm{R,T}}\int_{-\infty}^{\infty}\mathrm{d}\omega\ \omega a_\mu^\dagger(\omega)a_\mu(\omega)+\sum_{m,\mu}\int_{-\infty}^{\infty}\mathrm{d}\omega\ (\kappa_{m,\mu}(\omega)a_\mu^\dagger(\omega)\sigma_m+h.c.). \tag{S1}$$

Here, $\omega_m=\omega_0+\Delta_m$ denotes the transition frequency of the mth qubit, and $\sigma_m=|g_m\rangle\langle e_m|$ is its corresponding lowering operator. The operator $a_\mu(\omega)$ is the boson annihilation operator for a bath mode with frequency ω, where the subscript $\mu=\mathrm{T}$ (transmission) or R (reflection) distinguishes the mode. We assume weak inhomogeneity, namely, $|\Delta_m|\ll\omega_0$. In this regime, the coupling strengths satisfy $\kappa_{m,\mathrm{T/R}}(\omega)=\mathrm{g}_{m,,\mathrm{T/R}}\exp((-/+)i\omega x_m/c)\approx\mathrm{g}_{\mathrm{T/R}}\exp((-/+)i\omega x_m/c)$, so that the interaction strength for each qubit is approximately homogeneous, i.e., $|\kappa_{m,\mathrm{T/R}}(\omega)|\approx\mathrm{g}_{\mathrm{T/R}}$. The qubits are assumed to be equally spaced with separation d, so that $x_m=md$. For simplicity, we set $v_g=1$.

We first derive the master equation describing the time evolution of the system, which further supports the calculation of the field correlation function. The derivations mainly follow those in [1–3]. Following standard derivations, the Heisenberg equation for the field operator are obtained as

$$\dot{a}_\mathrm{T}(\omega,t)=-i\omega a_\mathrm{T}(\omega,t)-i\mathrm{g_T}e^{-i\omega x_m}\sigma_m(t),\qquad \dot{a}_\mathrm{R}(\omega,t)=-i\omega a_\mathrm{R}(\omega,t)-i\mathrm{g_R}e^{i\omega x_m}\sigma_m(t), \tag{S2}$$

which can be formally integrated as

$$a_\mathrm{T}(\omega,t)=e^{-i\omega(t-t_0)}a_\mathrm{T}(\omega,t_0)-i\mathrm{g_T}\sum_m\int_{t_0}^{t}e^{-i\omega(t-\tau)-i\omega x_m}\sigma_m(\tau)\,\mathrm{d}\tau\,,\quad a_\mathrm{R}(\omega,t)=-i\mathrm{g_R}\sum_m\int_{t_0}^{t}e^{-i\omega(t-\tau)+i\omega x_m}\sigma_m(\tau)\,\mathrm{d}\tau\,, \tag{S3}$$

where we have assumed that photons are injected from the left side of the waveguide, such that $a_\mathrm{R}(\omega,t_0)=0$. Consequently, the Heisenberg equations for the atomic operator are given by

$$\dot{\sigma}_m(t)=-i\omega_m\sigma_m(t)-i\sigma_m^z(t)\left(\int_{-\infty}^{\infty}\mathrm{g_T}a_\mathrm{T}(\omega,t)e^{i\omega x_m}\,\mathrm{d}\omega+\int_{-\infty}^{\infty}\mathrm{g_R}a_\mathrm{R}(\omega,t)e^{-i\omega x_m}\,\mathrm{d}\omega\right). \tag{S4}$$

Substituting the solutions of the field operators into the equations for the atomic operator, we have

$$\begin{aligned}\dot{\sigma}_m(t)=&-i\omega\sigma_m(t)-i\sigma_m^z(t)\Bigg(\mathrm{g_T}\int_{-\infty}^{\infty}e^{-i\omega(t-t_0)+i\omega x_m}a_\mathrm{T}(\omega,t_0)\,\mathrm{d}\omega\\&-i\mathrm{g_T^2}2\pi\sum_n\Theta(x_m-x_n)\sigma_n(t-|x_m-x_n|)-i\mathrm{g_R^2}2\pi\sum_n\Theta(x_n-x_m)\sigma_n(t-|x_m-x_n|)\Bigg)\\\approx&-i\omega\sigma_m(t)-i\sigma_m^z(t)\Bigg(\mathrm{g_T}\int_{-\infty}^{\infty}e^{-i\omega(t-t_0)+i\omega x_m}a_\mathrm{T}(\omega,t_0)\,\mathrm{d}\omega\\&-i\mathrm{g_T^2}2\pi\sum_n\Theta(x_m-x_n)\sigma_n(t)e^{i\omega_0|x_m-x_n|}-i\mathrm{g_R^2}2\pi\sum_n\Theta(x_n-x_m)e^{i\omega_0|x_m-x_n|}\sigma_n(t)\Bigg).\end{aligned}$$

In the last line, we have used the Markovian approximation

$$\sigma_n(t-|x_m-x_n|/c)\approx\sigma_n(t)e^{i\omega_n|x_m-x_n|/c}=\sigma_n(t)e^{i\omega_0(1+\Delta_n/\omega_0)|m-n|d/c}, \tag{S5}$$

and, for our purposes, we neglect the dependence of Δ_n in the phase factor, i.e.,

$$\sigma_n(t)e^{i\omega_n|x_m-x_n|/c}\approx\sigma_n(t)e^{i\omega_0|m-n|d/c}. \tag{S6}$$

This approximation is valid when the condition $|\Delta_n|/\omega_0\ll N^{-1}$ holds. Equivalently, this condition is satisfied if $\mathcal{C}W\ll\omega_0/N$, where $\mathcal{C}\sim\mathcal{O}(1)$ is a dimensionless constant. Specifically, for a detuning Δ_n drawn from a normal

distribution with standard deviation W, the inequality $|\Delta_n| \leq \mathcal{C}W$ is met with probability $\mathrm{erf}(\mathcal{C}/\sqrt{2})$. For instance, taking $\mathcal{C} = 2$ yields $\mathrm{erf}(\mathcal{C}/\sqrt{2}) \approx 0.95$, implying that the condition $|\Delta_n| \leq \mathcal{C}W$ is satisfies with near-unit probability. Thus, the approximation $|\Delta_n|/\omega_0 \ll N^{-1}$ holds with probability near unit (0.95), provided that $\mathcal{C}W \ll \omega_0/N$ is met.

Integrating the bath degrees of freedom, we have

$$\begin{aligned}\dot{\sigma}_m(t) = &-i\omega_m\sigma_m(t) - i\sqrt{\gamma_{\mathrm{T}}}\sigma_m^z(t)f(t-t_0,x_m)\\ &- \gamma_{\mathrm{T}}\sigma_m^z(t)\sum_n \sigma_n(t)\Theta(x_m-x_n)e^{i\omega_0|x_m-x_n|} - \gamma_{\mathrm{R}}\sigma_m^z(t)\sum_n \sigma_n(t)\Theta(x_n-x_m)e^{i\omega_0|x_m-x_n|},\end{aligned}$$

where $\gamma_{\mathrm{T/R}} = 2\pi \mathrm{g}_{\mathrm{T/R}}^2$ and $f(\tau, z)$ is defined by

$$f(\tau,z) = \frac{1}{\sqrt{2\pi}}\int_{-\infty}^{\infty} e^{-i\omega(\tau-z)}\,\mathrm{Tr}\left[\rho_E(t_0)a_{\mathrm{T}}(\omega,t_0)\right]\mathrm{d}\omega\,. \tag{S7}$$

Eq. (I) coincides with the equation of motion governed by the master equation

$$\dot{\rho} = -i((H_{\mathrm{eff}}+H_d)\rho - \rho(H_{\mathrm{eff}}^\dagger + H_d)) + \sum_{mn} 2(\gamma_{\mathrm{T}}\Theta(m-n)\cos(|m-n|\varphi) + \gamma_{\mathrm{R}}\Theta(n-m)\cos(|m-n|\varphi))\sigma_m\rho\sigma_n^\dagger, \tag{S8}$$

with

$$H_{\mathrm{eff}} = \sum_{m=1}^{N}\left(\Delta_m - \frac{i(\gamma_{\mathrm{nw}}+\gamma_{\mathrm{T}}+\gamma_{\mathrm{R}})}{2}\right)\sigma_m^\dagger\sigma_m - i\sum_{m>n}^{N}\left(\gamma_{\mathrm{T}}e^{i|m-n|\varphi}\sigma_m^\dagger\sigma_n + \gamma_{\mathrm{R}}e^{i|m-n|\varphi}\sigma_n^\dagger\sigma_m\right), \tag{S9}$$

and

$$H_d = \sum_m \sqrt{\gamma_{\mathrm{T}}}(f(t-t_0,md)\sigma_m^\dagger + h.c.), \tag{S10}$$

where $\varphi = \omega_0 d/v_g$.

The zero-time second-order photon correlations of the emitted field are defined as

$$g_\mu = \frac{\langle a_{\mu,\mathrm{out}}^\dagger(t)a_{\mu,\mathrm{out}}^\dagger(t)a_{\mu,\mathrm{out}}(t)a_{\mu,\mathrm{out}}(t)\rangle}{\langle a_{\mu,\mathrm{out}}^\dagger(t)a_{\mu,\mathrm{out}}(t)\rangle^2}, \tag{S11}$$

where $\langle\bullet\rangle$ denotes the expectation value over the emitted field. The input-output relations are given by

$$a_{\mathrm{T,out}}(t) = a_{\mathrm{T,in}}(t) - i\sqrt{\gamma_{\mathrm{T}}}\sum_m e^{-im\varphi}\sigma_m(t), \qquad a_{\mathrm{R,out}}(t) = -i\sqrt{\gamma_{\mathrm{R}}}\sum_m e^{im\varphi}\sigma_m(t), \tag{S12}$$

with

$$a_{\mathrm{T,in}}(t) = \frac{1}{\sqrt{2\pi}}\int_{-\infty}^{\infty} e^{-i\omega(t-t_0)}a_{\mathrm{T}}(\omega,t_0)\,\mathrm{d}\omega\,. \tag{S13}$$

Let us now consider a right-propagating coherent pulse as an input (drive), given by $\rho_E(t_0) \propto \exp(\alpha a_{\mathrm{T}}^\dagger(\omega_{\mathrm{in}}) - \alpha a_{\mathrm{T}}(\omega_{\mathrm{in}}))|0\rangle$, where the input pulse is assumed to be resonant with the transition frequency for the ordered system, i.e., $\omega_{\mathrm{in}} = \omega_0$. In the long-time limit, the properties of the emitted field are fully determined by the steady state ρ_{ss} of the qubits (in the rotating frame with respect to $H_0 = \omega_0\sum_m \sigma^\dagger\sigma_m$). By substituting the input-output relations into the definition of g_μ, one obtains

$$g_\mu = \frac{\mathrm{Tr}\left(\rho_{\mathrm{ss}}C_\mu^\dagger C_\mu^\dagger C_\mu C_\mu\right)}{\mathrm{Tr}\left(\rho_{\mathrm{ss}}C_\mu^\dagger C_\mu\right)^2}, \tag{S14}$$

where $C_{\mathrm{R}} = -i\sqrt{\gamma_{\mathrm{R}}}\sum_m e^{i\varphi m}\sigma_m$ and $C_{\mathrm{T}} = \alpha - i\sqrt{\gamma_{\mathrm{T}}}\sum_m e^{-i\varphi m}\sigma_m$, ρ_{ss} denotes the steady state corresponding to the master equation Eq. (S8) with $f(t-t_0,x_m) = \alpha e^{-i\omega_0(t-t_0)}e^{im\varphi}$. In the weak-input limit ($\alpha \ll 1$), one can solve for ρ_{ss} by neglecting quantum jumps, which yields the expansion $\rho_{\mathrm{ss}} \approx |G\rangle + \alpha|\psi^1\rangle + \alpha^2|\psi^2\rangle + \mathcal{O}(\alpha^3)$ [4].

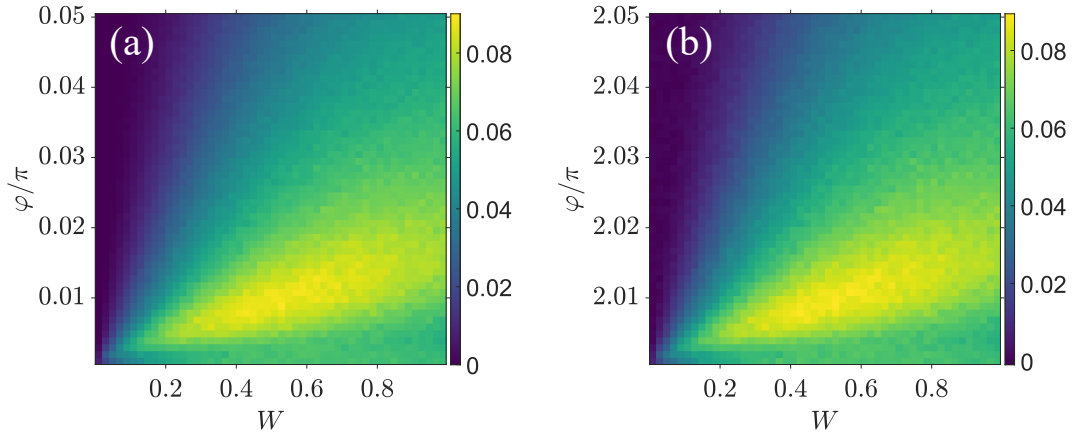

FIG. S1. (a) Probability of PA versus φ and W, where φ ranges from 0.001π to 0.05π. (b) Probability of PA versus φ and W, where φ ranges from 2.001π to 2.05π

.

Here, $|G\rangle = \bigotimes_{m=1}^{N} |g_m\rangle$, $|\psi^1\rangle = -(H_{\rm eff}^{(1)})^{-1} H_+ |G\rangle$ and $|\psi^2\rangle = -(H_{\rm eff}^{(2)})^{-1} H_+ |\psi^1\rangle$ are the single- and two-excitation components of the truncated steady-state, respectively, with $H_+ = \sqrt{\gamma_{\rm T}} \sum_m e^{im\varphi} \sigma_m^\dagger$. The operators $H_{\rm eff}^{(1)}$ and $H_{\rm eff}^{(2)}$ denote the single- and two-excitation subspace of the effective Hamiltonian $H_{\rm eff}$, respectively. After some calculations, one obtains for the transmitted field

$$g_{\rm T} = \frac{|1 - 2i\langle G|\tilde{C}_{\rm T}|\psi^1\rangle - \langle G|\tilde{C}_{\rm T}\tilde{C}_{\rm T}|\psi^2\rangle|^2}{|1 - i\langle G|\tilde{C}_{\rm T}|\psi^1\rangle|^4} + \mathcal{O}\big(|\alpha|^2\big), \tag{S15}$$

and for the reflected field

$$g_{\rm R} = \frac{\langle\psi^2|(\tilde{C}_{\rm R}^\dagger)^2(\tilde{C}_{\rm R})^2|\psi^2\rangle}{\langle\psi^1|\tilde{C}_{\rm R}^\dagger\tilde{C}_{\rm R}|\psi^1\rangle^2} + \mathcal{O}\big(|\alpha|^2\big), \tag{S16}$$

where $\tilde{C}_{\rm T} = \sqrt{\gamma_{\rm T}} \sum_m e^{-i\varphi m} \sigma_m$ and $\tilde{C}_{\rm R} = \sqrt{\gamma_{\rm R}} \sum_m e^{i\varphi m} \sigma_m$. These expressions can be further simplified as

$$g_{\rm T} = \frac{|1 - 2i\langle\phi_+^1|\psi^1\rangle - \langle\phi_+^2|\psi^2\rangle|^2}{|1 - i\langle\phi_+^1|\psi^1\rangle|^4}, \tag{S17}$$

and

$$g_{\rm R} = \frac{|\langle\phi_-^2|\psi^2\rangle|^2}{|\langle\phi_-^1|\psi^1\rangle|^4}, \tag{S18}$$

where $|\phi_\pm^1\rangle = \sqrt{\gamma_{\rm T}} \sum_m \exp(\pm im\varphi)\sigma_m^\dagger |G\rangle$ and $|\phi_\pm^2\rangle = 2\gamma_{\rm T} \sum_{m>n} \exp(\pm i(m+n)\varphi)\sigma_m^\dagger \sigma_n^\dagger |G\rangle$. When the coupling strengths to left- and right-going modes are homogeneous, i.e., $\gamma_{\rm T} = \gamma_{\rm R} = \gamma/2$, these equations, Eqs. (S17,S18), recover Eq. (2) of the main text.

We also emphasize the periodic nature of all the above derivations, including the master equation and the input-output relations, in the phase φ. Consequently, photon correlation should also be periodic in φ, with a period of 2π. Likewise, all the statistic quantities studied in the main text, such as the probability of PA and the probability density function, are also periodic in φ with period of 2π. For example, the probability of PA in the transmission for $N = 10$ (the inset of Fig. 2(a) in the main text) with $\varphi/\pi \in (0.001, 0.05)$, and that with $\varphi/\pi \in (2.001, 2.05)$, are shown in Fig. S1. The results show good agreements with each other.

II. ANALYTICAL CALCULATIONS OF $\mathbb{P}(s < 1)$ AND $P(0)$ FOR FEW-QUBIT SYSTEMS.

In this section, we present detailed calculations for the probabilities of PA and PPB for few-qubit systems, which further substantiate the results reported in the main text. The calculations for the transmission output and for the

reflection output with $\varphi = 0$ are carried out analytically, whereas those for the reflection output with $\varphi \neq 0$ are performed numerically.

A. Transmission

We first consider the single-qubit case. In this system, all two-photon scattering processes vanish, meaning that any terms involving $|\psi^2\rangle$ (or $\langle\psi^2|$) drop out. Since $H_{\text{eff}}^{(1)}$ is a 1×1 matrix in this case, the evaluation of $|\psi^1\rangle$ is straightforward. After some algebraic manipulations, the second-order correlation function is given by

$$g_{\text{T}} = \frac{(1+4\Delta_1^2)^2}{16\Delta_1^2}. \tag{S19}$$

Moreover, an analytical expression for the probability density function (PDF) corresponding to Eq. (S19) can be obtained. Specifically, the PDF is calculated as

$$P(s) = \frac{1}{\sqrt{2\pi}W}\int_{-\infty}^{\infty}\delta\left(\frac{(1+4\Delta_1^2)^2}{16\Delta_1^4} - s\right)e^{-\Delta_1^2/2W^2}\,\mathrm{d}\Delta_1. \tag{S20}$$

Here, the Dirac delta function is handled using the standard identity $\delta(f(x)) = \sum_j \delta(x - x_j)/|f'(x_j)|$. After some calculations, one finds that $P(s) = 0$ for $s < 1$. Thus, we have

$$\mathbb{P}(s < 1) = P(0) = 0. \tag{S21}$$

For $s \geq 1$, the PDF is given by

$$P(s) = \frac{1}{4\sqrt{2\pi}W}\frac{1}{(\sqrt{s}-1)^{3/2}\sqrt{s}}e^{1/(1-1\sqrt{s})8W^2}. \tag{S22}$$

The asymptotic behaviors for $P(s > 1)$ are

$$P(s \to 1^+) \sim \frac{1}{4\pi W}(s-1)^{-3/2}e^{-1/(4W^2(s-1))}, \qquad P(s \to +\infty) \sim \frac{1}{4\sqrt{2}\pi W}s^{-5/4}. \tag{S23}$$

Furthermore, the mode of the PDF, corresponding to the most probable value of the correlation function, is located at

$$s_{\max} = \frac{1 + 56W^2 + 464W^4 + \sqrt{W^8(1+28W^2)^2(1+56W^2+464W^4)}}{800W^4}, \tag{S24}$$

This result shows that the mode scales as $s_{\max} \sim W^{-4}$ for $W \to 0^+$ and $s_{\max} \sim 1$ for $W \to +\infty$. In other words, when $W \ll 1$ the most probable output is strongly bunched, while for $W \gg 1$ it is nearly coherent.

For a two-qubit system, although the analytical expression become more involved, the calculation remains tractable. In this case, the correlation function is given by

$$g_{\text{T}} = \frac{(8\Delta_1^2\Delta_2^2 + f_+ - \cos(2\varphi))\big(8\Delta_1^2\Delta_2^2(1+(\Delta_1+\Delta_2)^2) + (\Delta_1+\Delta_2)^2(f_- - \cos(\varphi)) + 4\Delta_1\Delta_2(\Delta_1+\Delta_2)\sin(2\varphi)\big)}{64\Delta_1^4\Delta_2^4(1+(\Delta_1+\Delta_2)^2)}, \tag{S25}$$

with $f_\pm = 1 + 2\Delta_1^2 + 2\Delta_2^2 \pm 4\Delta_1\Delta_2\cos(2\varphi) - 2(\Delta_1+\Delta_2)\sin(2\varphi)$. It is practically infeasible to derive a closed-form expression for the corresponding PDF in this case. Nonetheless, since the correlation function $g_{\text{T}} \geq 1$, we have $\mathbb{P}(s < 1) = 0$ and $P(0) = 0$.

B. Reflection

For the single-qubit system, the absence of two-photon scattering processes implies that $\langle\phi_-^2|\psi^2\rangle = 0$, so that $g_{\text{R}} = 0$. For the two-qubit system, we first consider the case $\varphi = 0$. In this situation, the correlation function reduces

to

$$g_{\mathrm{R}} = \frac{(\Delta_1+\Delta_2)^2 + 4\Delta_1^2\Delta_2^2}{(\Delta_1+\Delta_2)^2 + (\Delta_1+\Delta_2)^4}. \tag{S26}$$

The probability of PA is then calculated from

$$\mathbb{P}(s<1) = \int_0^1 P(s)\mathrm{d}s = \frac{1}{2\pi W^2}\int_{-\infty}^{\infty}\mathrm{d}\Delta_1\int_{-\infty}^{\infty}\mathrm{d}\Delta_2\ \exp\!\left(-\frac{\Delta_1^2+\Delta_2^2}{2W^2}\right)\Theta(g_{\mathrm{R}}-1), \tag{S27}$$

where $\Theta(x)$ denotes the Heaviside step function. Changing the variables as $2\Omega = \Delta_1+\Delta_2$ and $2\Lambda = \Delta_1-\Delta_2$, one obtains $g_{\mathrm{R}} = (\Omega^2+(\Omega^2-\Lambda^2)^2)/(\Omega^2+4\Omega^4)$. PA occurs when

$$|\Omega| > \frac{1}{\sqrt{3}}|\Lambda|. \tag{S28}$$

It follows that the probability of PA is given by

$$\mathbb{P}(s<1) = \frac{1}{\pi W^2}\iint_{|\Omega|>\frac{|\Lambda|}{\sqrt{3}}}\mathrm{d}\Omega\mathrm{d}\Lambda\ \exp\!\left(-\frac{\Omega^2+\Lambda^2}{W^2}\right) = \frac{2}{3}, \tag{S29}$$

which recovers the equality stated in Eq.(4) of the main text. To demonstrate the result $P(0)=0$ presented in the main text, we now analyze the asymptotic behavior of $P(s)$ for $s \ll 1$. Starting from

$$P(s) = \frac{4}{\pi W^2}\int_0^{\infty}\mathrm{d}\Omega\int_0^{\infty}\mathrm{d}\Lambda\ \exp\!\left(-\frac{\Omega^2+\Lambda^2}{W^2}\right)\delta\!\left(\frac{\Omega^2+(\Omega^2-\Lambda^2)^2}{\Omega^2+4\Omega^4}-s\right). \tag{S30}$$

a change of variables $\Omega^2\to\Omega$ and $\Lambda^2\to\Lambda$ yields

$$P(s) = \frac{1}{\pi W^2}\int_0^{\infty}\mathrm{d}\Omega\int_0^{\infty}\mathrm{d}\Lambda\ \frac{1}{\sqrt{\Omega\Lambda}}\exp\!\left(-\frac{\Omega+\Lambda}{W^2}\right)\delta\!\left(\frac{\Omega+(\Omega-\Lambda)^2}{\Omega+4\Omega^2}-s\right). \tag{S31}$$

Carrying out the integral over Λ leads to

$$P(s) = \frac{1}{\pi W^2}\int_{(1-s)/4s}^{\infty}\mathrm{d}\Omega\ \exp\!\left(-\Omega/W^2\right)\frac{(1+4\Omega)}{\sqrt{4s\Omega+s-1}}\left[\frac{\exp\!\left(\frac{-\Omega_+}{W^2}\right)}{\sqrt{\Omega_+}}+\frac{\exp\!\left(\frac{-\Omega_-}{W^2}\right)}{\sqrt{\Omega_-}}\right], \tag{S32}$$

where $\Omega_\pm = \Omega \pm \sqrt{\Omega(4s\Omega+s-1)}$. In the limit $s \ll 1$, the lower limit of the Ω integral can be approximated as $(1-s)/4s \approx 1/4s$. In this regime, one can approximate $\Omega_\pm \approx \Omega$ and $\sqrt{4s\Omega+s-1} \approx \sqrt{4s\Omega-1}$. With these approximations, the expression simplifies to

$$P(s) \approx \frac{2}{\pi W^2\sqrt{s}}\int_{1/4s}^{\infty}\mathrm{d}\Omega\ e^{-2\Omega/W^2}\frac{1}{\sqrt{4s\Omega-1}}. \tag{S33}$$

This asymptotic form reveals that strong photon antibunching ($g_{\mathrm{R}} \ll 1$) is associated with large detuning, as dictated by the lower integration bound $\Omega = \Delta_1+\Delta_2 > 1/4s \sim s^{-1}$. Performing the integral over Ω yields

$$P(s\ll 1) \sim \frac{1}{\sqrt{2\pi}W}s^{-1}\exp\!\left(-\frac{1}{2W^2 s}\right). \tag{S34}$$

From this expression it is evident that as $s\to 0$, $P(s)\to 0$; hence, $P(0)=0$, in agreement with the result stated in the main text. Finally, we compare this analytical approximation to numerical integration of the starting expression (Eq. (S30)) [see Figs. S2(a-c)].

For the system with $\varphi \neq 0$, the correlation function is given by

$$g_{\mathrm{R}} = \left|\frac{(-i+ie^{2i\varphi}+2\Delta_1+2\Delta_2)(e^{2i\varphi}+(2\Delta_1-i)(2\Delta_2-i))}{(\Delta_1+\Delta_2-i)(2\Delta_2-i+e^{2i\varphi}(2\Delta_1+i))^2}\right|^2. \tag{S35}$$

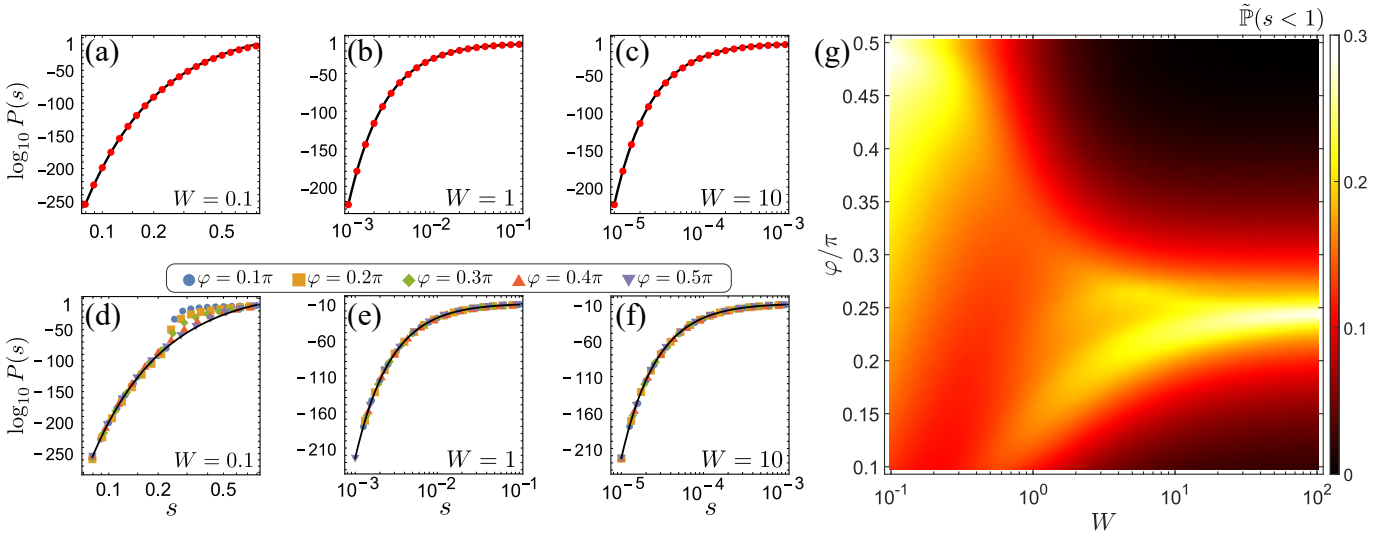

FIG. S2. (a-c) The asymptotic behaviors of $P(s)$. The chosen disorder strengths are $W = 0.1$ (a), $W = 1$ (b), and $W = 10$ (c). In all plots, red dots are obtained from the numerical integration of Eq. (S30), and black lines represent the analytical solutions from Eq. (S34). (d-f) The asymptotic behaviors of $P(s)$. The chosen disorder strengths are $W = 0.1$ (d), $W = 1$ (e), and $W = 10$ (f). The different symbols correspond to systems with different values of φ. In all plots, the symbols are obtained from the numerical integration with the correlation expression replaced by Eq. (S35), and black lines represent the analytical solutions from Eq. (S34). (g) $\tilde{\mathbb{P}}(s < 1) = \mathbb{P}(s < 1) - 2/3$ versus phase and disorder strength. The result is obtained from numerical integration of Eq. (S27), while the expression of correlation is replaced by Eq. (S35)

.

g_{T}	Δ_1	Δ_2	Δ_3
10^{-8}	0.149124450372206	−0.053903424589490	0.144085703957167
10^{-10}	0.148134188883455	−0.055253952848190	0.144762975264912
10^{-12}	0.149005562567387	−0.054129160721382	0.144182673551411

TABLE S1. Partial solutions $\{\Delta_1, \Delta_2, \Delta_3\}$ of equation $g_{\mathrm{T}} = s_0$ with $s_0 = 10^{-8}, 10^{-10}, 10^{-12}$. Here $\varphi = 0.04\pi$, which is the same with the parameters in Fig. 1(c) of main text.

In this case, the analytical forms for both $\mathbb{P}(s < 1)$ and $P(0)$ are practically infeasible to obtain. Fig. S2(g) displays the numerical results for $\mathbb{P}(s < 1)$, which now depend on both the phase and the disorder strength. Notably, the numerical data imply that $\mathbb{P}(s < 1)$ is bounded from below by 2/3, the value obtained in the Dicke limit for a two-qubit system. As the disorder strength increases, $\mathbb{P}(s < 1)$ attains a maximum at $\varphi \sim 0.25\pi$, and then saturates to the lower bound of 2/3 when $\varphi \sim 0$ or 0.5π.

Regarding $P(0)$, Figs. S2(d-f) illustrate the asymptotic behavior of $P(s)$ for $s \ll 1$. It is evident that $P(s \ll 1)$ displays essentially the same asymptotic form as in the case of $\varphi = 0$. This similarity arises because strong PA is primarily associated with samples $\{\Delta_1, \Delta_2\}$ in which one detuning $|\Delta_i| \ll 1$ (i.e., nearly resonant), while the other $|\Delta_{j\neq i}| \gg 1$ (i.e., far off-resonant). Physically, this scenario corresponds to one qubit interacting strongly with the input while the other is nearly transparent to it, effectively reducing the system to a single-photon absorber/emitter. However, since the detunings are sampled from a Gaussian distribution, the probability of obtaining $|\Delta_{j\neq i}| \gg 1$ decreases exponentially with $|\Delta_{j\neq i}|$, which ultimately leads to an exponential decay of $P(s)$ as $s \to 0$. Consequently, $P(0) = 0$ is recovered in this regime.

These findings demonstrate that, even when $\varphi \neq 0$, the essential asymptotic behavior of the correlation function remains consistent with the $\varphi = 0$ case, while the overall probability $\mathbb{P}(s < 1)$ exhibits a nontrivial dependence on both the phase and the disorder strength.

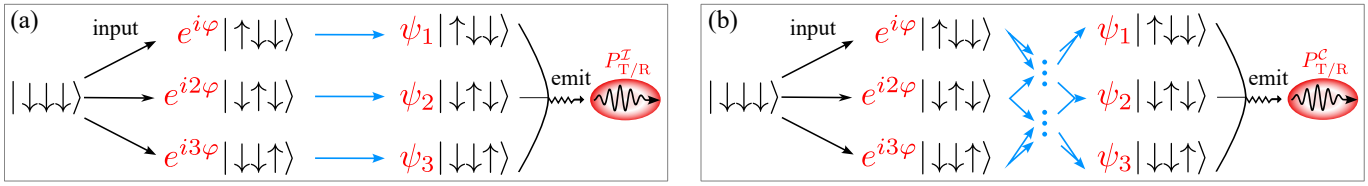

FIG. S3. (a-b) Schematics of single-photon scattering path involves (a) non-interacting path (b) interacting path for an array with $N = 3$.

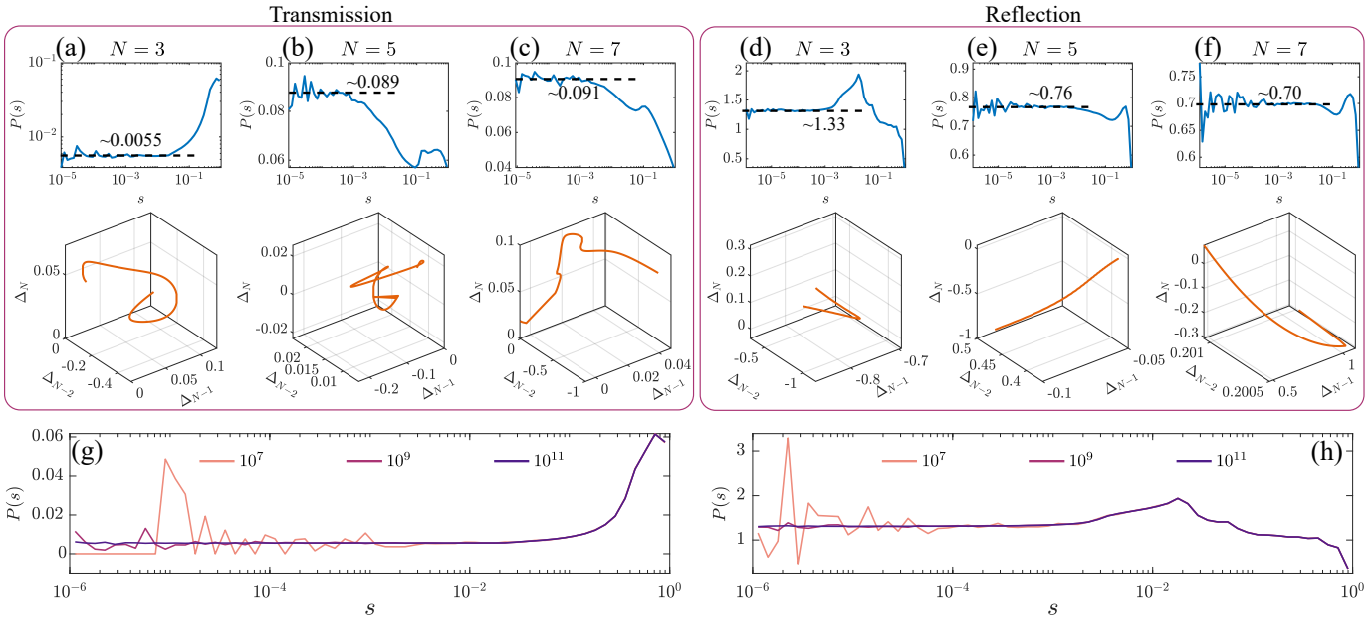

FIG. S4. (a-c) Top: PDFs; Bottom: Solutions of $g_{\rm T} = 10^{-10}$ for the transmission output. The chosen parameters are $\varphi = 0.01\pi$ and $W = 0.15$; the chain sizes are indicated above the plots. (d-f) Top: PDFs; Bottom: Solutions of $g_{\rm R} = 10^{-10}$ for the reflection output. The chosen system parameters are $\varphi = 0.5\pi$ and $W = 1$; the chain sizes are indicated above the plots. In the top of (a-f), the results are obtained from 10^9 disorder realizations. (g-h) PDFs for the transmission (g) and reflection (h) outputs under different numbers of disorder realizations. The chosen parameters are $N = 3$, $\varphi = 0.01\pi$, $W = 0.15$ in (g) and $N = 3$, $\varphi = 0.5\pi$, $W = 1$ in (h).

III. PHYSICAL MECHANISM OF NPPB

Although the solutions presented in the main text correspond to $g_{\rm T} = 10^{-10}$, one can also obtain solutions for $g_{\rm T} = \epsilon$, where ϵ can be made arbitrarily close to 0 as computational precision increases. To achieve an NPPB event, i.e., $g_{\rm T/R} = \epsilon \to 0$, the detunings of the qubits must be very finely tuned (see Table. S1 for an example). This requirement for fine-tuning of parameters for an NPPB event suggests that the underlying physical mechanism is the destructive interference of quantum paths [5, 6].

To manifest the interference effect, note that the photon correlations depend solely on the single- and two-photon scattering processes. Consequently, the overall quantum path comprises three contributions: (i) a single-photon scattering path with probability amplitude $\langle\phi_{\pm}^1|\psi^1\rangle$; (ii) a two-photon scattering path with probability amplitude $\langle\phi_{\pm}^2|\psi^2\rangle$; (iii) a free propagation path with probability amplitude 1. From Eqs. (S17-S18), NPPB in the transmission output involves nearly completely destructive interference among the single-photon scattering path, the two-photon scattering path, and the free propagation path, whereas NPPB in the reflection output involves nearly completely destructive interference solely of the two-photon scattering path. Furthermore, the single- and two-photon scattering paths are determined by transition paths, which are governed by the non-Hermitian effective Hamiltonian $H_{\rm eff}$. These transition paths dictate how the qubits are excited by the input and how the emitted photons interfere with each other.

More specifically, in the single-photon scattering path the fully inverted chain of qubits is first excited by the input to the state, $|G\rangle + \alpha H_+|G\rangle$. Then, the single-excitation component, $\alpha H_+|G\rangle \propto \sum_m \exp(im\varphi)\sigma_m^\dagger|G\rangle$, transitions to

the steady state through an infinite number of transition paths. To see this, we can rewrite

$$|\psi^1\rangle = -(H_{\text{eff}}^{(1)})^{-1}H_+|G\rangle = \lim_{z\to 0}\frac{1}{z-H_{\text{eff}}^{(1)}}H_+|G\rangle = \lim_{z\to 0}(G_{\mathcal{I}}^{(1)}(z)+G_{\mathcal{C}}^{(1)}(z))H_+|G\rangle, \tag{S36}$$

with

$$G_{\mathcal{I}}^{(1)}(z) = \frac{1}{z-H_0^{(1)}}, \qquad G_{\mathcal{C}}^{(1)}(z) = \sum_{j=1}^{\infty} G_{\mathcal{C},j}^{(1)}(z), \qquad G_{\mathcal{C},j}^{(1)}(z) = \left(G_{\mathcal{I}}^{(1)}(z)T^{(1)}\right)^j G_{\mathcal{I}}^{(1)}(z). \tag{S37}$$

Here $H_0 = \sum_m(\Delta_m - i\gamma/2)\sigma_m^\dagger\sigma_m$ and $T = -i\gamma\sum_{m\neq n}\exp(i\varphi|m-n|)\sigma_m^\dagger\sigma_n/2$ represent the free and interaction terms of the non-Hermitian Hamiltonian, respectively; the superscript (1) denotes the single-excitation sector. Now, assuming that the single-excitation component of the steady state can be written as $|\psi^1\rangle = \sum_m \psi_m\sigma_m^\dagger|G\rangle$, the unnormalized probability amplitude is given by $\psi_m = \psi_m^{\mathcal{I}} + \psi_m^{\mathcal{C}}$, with

$$\psi_m^{\mathcal{I}} = \lim_{z\to 0}\langle G|\sigma_m G_{\mathcal{I}}^{(1)}(z)H_+|G\rangle = -\sqrt{\frac{\gamma}{2}}\frac{e^{im\varphi}}{\Delta_m - i\gamma/2}, \qquad \psi_m^{\mathcal{C}} = -\sqrt{\frac{\gamma}{2}}\lim_{z\to 0}\sum_{n=1}^{N}\sum_{j=1}^{\infty}e^{in\varphi}\langle G|\sigma_m G_{\mathcal{C},j}^{(1)}(z)\sigma_n^\dagger|G\rangle. \tag{S38}$$

The first term, $\psi_m^{\mathcal{I}}$, represents the steady-state probability amplitude of qubits individually interacting with the waveguide, while the second term, $\psi_m^{\mathcal{C}}$, represents the probability amplitude for qubits collectively interacting with the waveguide. This collective term involves transitions between different qubits mediated by the long-range interaction of photons. Such transitions can be viewed as an emission-reabsorption process, whereby photons emitted by one qubit are reabsorbed by another. Specifically, for the n-th qubit initially excited by the input, the excitation transfers to the m-th qubit through an infinite sequence of transitions, with the unnormalized probability amplitudes for the j-th path given by $e^{in\varphi}\sqrt{\gamma/2}\langle G|\sigma_m G_{\mathcal{C},j}^{(1)}(z)\sigma_n^\dagger|G\rangle$.

After excitation, each excited qubit in the state $\psi_m\sigma_m^\dagger|G\rangle$ can emit a single photon into the waveguide with an (unnormalized) probability amplitude ψ_m. The propagation of this emitted photon acquires a phase factor $\exp(\pm im\varphi)$, where the minus (plus) sign corresponds to the transmission (reflection) output. Consequently, the final probability amplitude for the single-photon path is given by

$$\langle \sup_\pm^1|\psi^1\rangle = P_{\text{T/R}}^{\mathcal{I}} + P_{\text{T/R}}^{\mathcal{C}}, \tag{S39}$$

with

$$P_{\text{T/R}}^{\mathcal{I}} = -\frac{\gamma}{2}\sum_{m=1}^{N}\frac{\exp[(0/2)im\varphi]}{\Delta_m - i\gamma/2}, \qquad P_{\text{T/R}}^{\mathcal{C}} = \sqrt{\frac{\gamma}{2}}\lim_{z\to 0}\sum_{m=1}^{N}\sum_{j=1}^{\infty}\exp[(-/+)im\varphi]\langle G|\sigma_m G_{\mathcal{C},j}^{(1)}(z)H_+|G\rangle. \tag{S40}$$

The first term, $P_{\text{T/R}}^{\mathcal{I}}$, involves only a sum over the qubit index. It represents the superposition of N paths in which the m-th path corresponds to a photon emitted from the m-th qubit propagating along the waveguide without being reabsorbed by other qubits; we refer to this term as the probability amplitude of the "non-interacting transition path". Consequently, the second term, $P_{\text{T/R}}^{\mathcal{C}}$, represents the probability amplitude for the case in which the emitted photon can be reabsorbed by other qubits, and we refer to it as "interacting transition path". Thus, the final probability amplitude for the single-photon scattering path, $\langle\phi_\pm^1|\psi^1\rangle$, is the combination of the non-interacting path and interacting paths. In Fig. S3, we present the single-photon scattering processes for an array with $N = 3$ as an example.

As for the two-photon scattering path, the conclusion is similar. In addition to the single-photon events, the two-photon scattering path, $\langle\phi_\pm^2|\psi^2\rangle$, further involves the two-excitation steady state of the qubit ensemble. After similar derivations, the probability amplitude for the two-photon scattering path can be expressed as

$$\langle \sup_\pm^2|\psi^2\rangle = P_{\text{T/R}}^{\mathcal{II}} + P_{\text{T/R}}^{\mathcal{IC}} + P_{\text{T/R}}^{\mathcal{CI}} + P_{\text{T/R}}^{\mathcal{CC}}, \tag{S41}$$

with

$$\begin{cases} P_{\mathrm{T/R}}^{\mathcal{II}} = \dfrac{\gamma^2}{2}\displaystyle\sum_{m>n}\frac{\exp[(0/2)i(m+n)\varphi]}{(\Delta_m - i\gamma/2)(\Delta_n - i\gamma/2)} \\ P_{\mathrm{T/R}}^{\mathcal{IC}} = \gamma\lim\limits_{z\to 0}\displaystyle\sum_{m>n}\sum_{j=1}^{\infty}\exp[(-/+)i(m+n)\varphi]\langle G|\sigma_m\sigma_n G_{\mathcal{I}}^{(2)}(z)H_+ G_{\mathcal{C},j}^{(1)}(z)H_+|G\rangle \\ P_{\mathrm{T/R}}^{\mathcal{CI}} = \gamma\lim\limits_{z\to 0}\displaystyle\sum_{m>n}\sum_{j=1}^{\infty}\exp[(-/+)i(m+n)\varphi]\langle G|\sigma_m\sigma_n G_{\mathcal{C},j}^{(2)}(z)H_+ G_{\mathcal{I}}^{(1)}(z)H_+|G\rangle \\ P_{\mathrm{T/R}}^{\mathcal{CC}} = \gamma\lim\limits_{z\to 0}\displaystyle\sum_{m>n}\sum_{j,k=1}^{\infty}\exp[(-/+)i(m+n)\varphi]\langle G|\sigma_m\sigma_n G_{\mathcal{C},j}^{(2)}(z)H_+ G_{\mathcal{C},k}^{(1)}(z)H_+|G\rangle \end{cases}. \tag{S42}$$

Similarly, the first term $P_{\mathrm{T/R}}^{\mathcal{II}}$ denotes the probability amplitude of the non-interacting path, while the remaining terms correspond to the probability amplitudes of the interacting path. As a consequence, NPPB in the transmission output involves nearly completely destructive interference among the single-photon scattering path with a probability amplitude $\langle\phi_+^1|\psi^1\rangle$, the two-photon scattering path with a probability amplitude $\langle\phi_+^2|\psi^2\rangle$, and the free propagation path with a probability amplitude 1; whereas NPPB in the reflection output involves nearly completely destructive interference solely of the two-photon scattering path with a probability amplitude $\langle\phi_-^2|\psi^2\rangle$.

In addition to the physical mechanism of NPPB, the mathematical structure of solutions satisfying $g_{\mathrm{T/R}} = 0$ is somewhat subtle. For an array of N qubits, the solutions for $g_{\mathrm{T/R}} = 0$ form a $(N-2)$-dimensional submanifold. This is because, these solutions are essentially constrained by two conditions

$$g_{\mathrm{T/R}} = 0, \qquad \boldsymbol{\nabla} g_{\mathrm{T/R}} = \mathbf{0}. \tag{S43}$$

The second condition arises from the fact that the correlation function is analytical and attains its minimum value at 0; hence, its gradient must vanish at 0. Consequently, solutions of $g_{\mathrm{T/R}} = \epsilon$ with $\epsilon \neq 0$ form a $(N-1)$-dimensional submanifold, since only the condition $g_{\mathrm{T/R}} = \epsilon$ is imposed. However, as the value of ϵ decreases toward 0, one can expect that this $(N$–$1)$-dimensional submanifold nearly collapses into a $(N$–$2)$-dimensional submanifold, corresponding to the solutions of $g_{\mathrm{T/R}} = 0$. As a result, solutions of $g_{\mathrm{T}} = 10^{-10}$ for an array with $N = 3$ form near a curve embedded in the 3D parameters space, as shown in the main text. In Fig. S4, we present solutions of the correlation functions for chains with $N \geq 3$. The solutions are obtained as follows: (i) For $N = 3$, we first use a nonlinear programming solver to find the maximum value of $\sum_m \Delta_m^2$, the set $\{\Delta_{1,\min},\ \Delta_{2,\min},\ \Delta_{3,\min}\}$, under the constraint $g_{\mathrm{T/R}} = 10^{-10}$. That is,

$$g_{\mathrm{T/R}}\big|_{\Delta_1=\Delta_{1,\min},\Delta_2=\Delta_{2,\min},\Delta_3=\Delta_{3,\min}} = 10^{-10}, \qquad \sum_m \Delta_m^2\big|_{\Delta_1=\Delta_{1,\min},\Delta_2=\Delta_{2,\min},\Delta_3=\Delta_{3,\min}} = \min\left\{\sum_m \Delta_m^2\right\}. \tag{S44}$$

Based on this solution, we then apply the Gauss-Newton algorithm to automatically find solutions to the equation $g_{\mathrm{T/R}} = 10^{-10}$ until a maximum number of solutions, K_{sols}, is reached. Here, we set $K_{\mathrm{sols}} = 10^5$. (ii) For $N > 3$, we similarly find the minimum of $\sum_m \Delta_m^2$ under the constraints $g_{\mathrm{T/R}} = 10^{-10}$; while in the Gauss-Newton algorithm, we fix the first $(N-3)$ detunings and solve the equation $g_{\mathrm{T/R}} = 10^{-10}$ for the last three detunings. Due to the existence of NPPB, the PDF tends to be constant at $s \ll 1$, with fluctuations near that constant, as shown in Figs. S4(a-f). These fluctuations arise from the standard deviation inherent in the numerical method used to estimate the PDF, and they can be effectively suppressed by increasing the number of disorder realizations [see Figs. S4(g-h)]. Details regarding the numerical method are discussed in the last section.

IV. CORRELATION FUNCTION IN THE WEAK- AND STRONG-DISORDER LIMITS

A. Weak-disorder limit ($W \ll 1$)

In the weak-disorder limit, one can expect that the photon correlations do not deviate significantly from their clean counterparts. This means that for the reflection output, the correlation functions are expected to be distributed around the value of g_{R} for $W = 0$ [see Fig. S5(a)]; while for the transmission output, the correlation functions are expected to be distributed around $g_{\mathrm{T}} \sim +\infty$. To confirm this statement, we present the PDFs in Figs. S5(b-i). For the

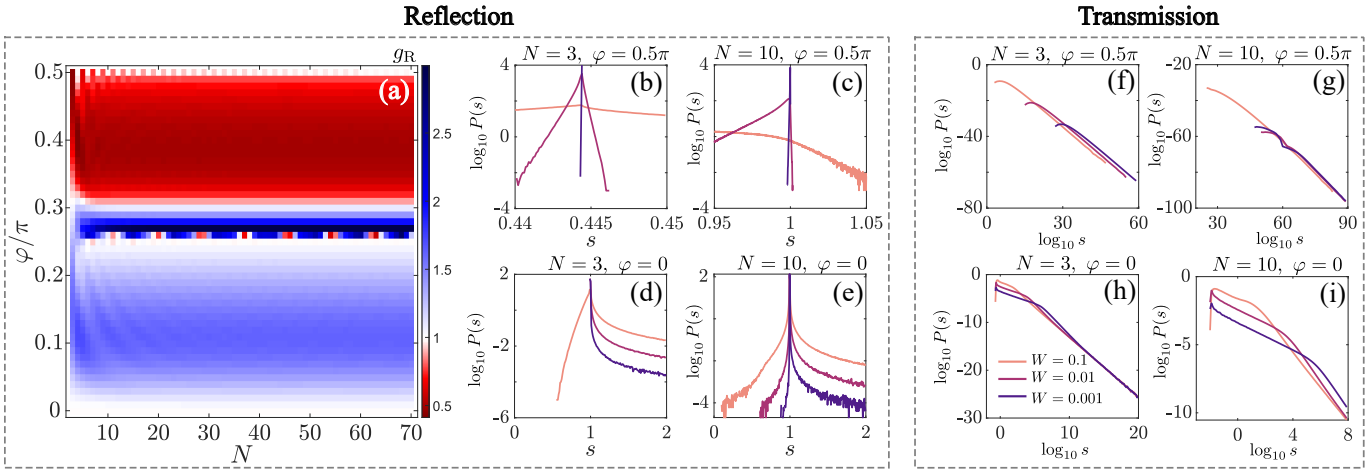

FIG. S5. (a) Correlation functions for the reflection output in the absence of disorder. (b-e) PDFs for the reflection output versus disorder strength. Parameters are indicated above the plots. (f-i) PDFs for the reflection output versus disorder strength. Parameters are the same as (b-e). In all plots, the results are obtained from 10^7 disorder realizations.

reflection output [see Figs. S5(f-i)], the shapes of $P(s)$ become increasingly sharper around $\{1, 0.444, 1, 1\}$, as disorder strength decreases. The peaks of the PDFs correspond to the values of the correlation function in the clean limit ($W = 0$). For the transmission output, as the disorder strength decreases, when $\varphi = 0.5\pi$ the region where $P(s) \neq 0$ shifts further towards infinity; and when $\varphi = 0$, the value of $P(s)$ decreases for smaller s while it increases for larger s [see Figs. S5(b-e)]. Both of these results indicate that g_T in the weak-disorder limit is distributed around infinity.

B. Strong-disorder limit ($W \gg 1$)

In the strong-disorder limit, one can expect that the photon-mediated interaction between qubits is significantly quenched [see Fig. S6(a)]. This indicates that the probability amplitudes of interacting paths are extremely suppressed, so that one can consider only the probability amplitudes of non-interacting paths. In this situation, the correlation functions can be solved exactly, as derived in the previous section. After some calculations, the truncated steady states are given by

$$|\tilde{\psi}^1\rangle = -\frac{\gamma}{2}\sum_{m=1}^{N}\frac{\exp(im\varphi)}{\Delta_m - i\gamma/2}\sigma_m^\dagger|G\rangle, \qquad |\tilde{\psi}^2\rangle = |\tilde{\psi}^1\rangle \otimes |\tilde{\psi}^1\rangle = \frac{\gamma^2}{2}\sum_{m>n}\frac{\exp(i(m+n)\varphi)}{(\Delta_m - i\gamma/2)(\Delta_n - i\gamma/2)}\sigma_m^\dagger\sigma_n^\dagger|G\rangle. \tag{S45}$$

Thus,

$$g_T = \frac{|1 - 2iP_T^{\mathcal{I}} - P_T^{\mathcal{I}\mathcal{I}}|^2}{|1 - iP_T^{\mathcal{I}}|^4} = \frac{|1 + i\sum_m(\Delta_m - i/2)^{-1} - \sum_{m>n}(\Delta_m - i/2)^{-1}(\Delta_n - i/2)^{-1}/2|^2}{|1 + i\sum_m(\Delta_m - i/2)^{-1}/2|^4} \tag{S46}$$

and

$$g_R = \frac{|P_R^{\mathcal{I}\mathcal{I}}|^2}{|P_R^{\mathcal{I}}|^4} = \frac{|2\sum_{m>n}\frac{e^{2i(m+n)\varphi}}{(\Delta_m - i/2)(\Delta_n - i/2)}|^2}{|\sum_m \frac{e^{2im\varphi}}{\Delta_m - i/2}|^4}. \tag{S47}$$

From Eq. (S46), the correlation function in the transmission output is independent of the distance between qubits, i.e., independent of φ. In addition, solutions of $g_T = 0$ exist when $\varphi = 0$, provided that $N \geq 3$. For instance, one can easily verify that $g_T = 0$ if $\Delta_i = 1/2$ and $\Delta_j = -1/2$ for $i \neq j$. However, these results do not contradict those obtained from Eq. (S15), where the correlation functions are distance-dependent and have no solutions satisfying $g_T = 0$ when $\varphi = 0$. This discrepancy arises because Eqs. (S46,S47) are valid only in the sense of disorder averaging.

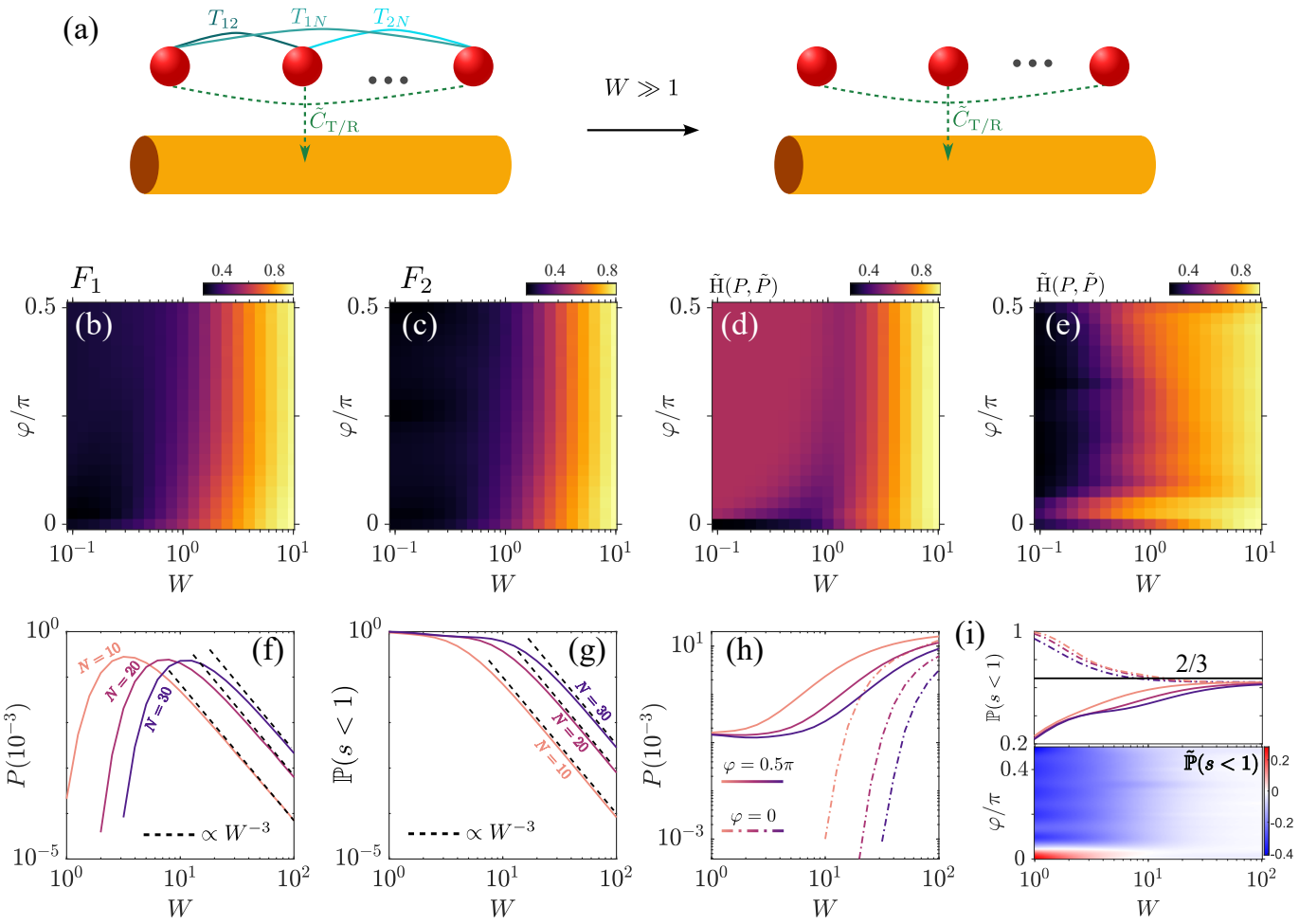

FIG. S6. (a) Schematics of the systems in the weak- and intermediate-disorder regimes (left panel); and in the strong-disorder regime (right panel). Here $T_{mn} = -i\exp(i|m-n|\varphi)\sigma_m^\dagger\sigma_n/2$ with $m \neq n$. (b,c) Fidelity between the truncated steady state $\{|\psi^1\rangle, |\psi^2\rangle\}$ obtained from the non-Hermitian Hamiltonian with long-range interactions and the truncated steady state $\left\{|\tilde{\psi}^1\rangle, |\tilde{\psi}^2\rangle\right\}$ obtained from Eq. (S45). (d,e) Hellinger distance between the PDFs obtained from Eqs. (S15-S16) and those obtained from Eqs. (S46,S47). Here we plot $\tilde{\mathrm{H}}(P,\tilde{P}) = 1 - \tilde{\mathrm{H}}(P,\tilde{P})$. $N = 10$ in plots (b-e). The results are obtained from 10^4 disorder realizations. (f,g) Probability of PA and $P(10^{-3})$ for the transmission output versus disorder strength for different system sizes. The dashed lines indicate slopes of W^{-3}. These results are obtained from Eq. (S46) using 10^{10} disorder realizations. (h,i) Probability of PA and $P(10^{-3})$ for the reflection output versus disorder strength for different system sizes and phases. These results are obtained from Eq. (S47) using 10^{10} disorder realizations. Different colored lines correspond to different chain sizes (the same as those in (f,g)). In the top panel of (i), the parameters are the same as in (h) (labeled within the plot), and in the bottom panel of (i), we plot $\mathbb{P}(s<1) - 2/3$ for $N = 10$.

To examine the validity of Eqs. (S46,S47), we numerically calculate the normalized fidelity

$$F_1 = \frac{|\langle\tilde{\psi}^1|\psi^1\rangle|}{\sqrt{|\langle\tilde{\psi}^1|\tilde{\psi}^1\rangle||\langle\psi^1|\psi^1\rangle|}}, \qquad F_2 = \frac{|\langle\tilde{\psi}^2|\psi^2\rangle|}{\sqrt{|\langle\tilde{\psi}^2|\tilde{\psi}^2\rangle||\langle\psi^2|\psi^2\rangle|}}. \tag{S48}$$

Since photon correlations are fully encoded in the truncated steady states, the closer the normalized fidelity is to unity, the closer the values of the two types of correlation functions (obtained from Eqs. (S15,S16) and Eqs. (S46,S47)) will be. We also investigate the Hellinger distance between the PDFs $P(s)$ obtained from Eqs. (S15-S16) and the PDFs $\tilde{P}(s)$ obtained from Eqs. (S46,S47). The Hellinger distance between two probability density functions, $q(x)$ and $p(x)$,

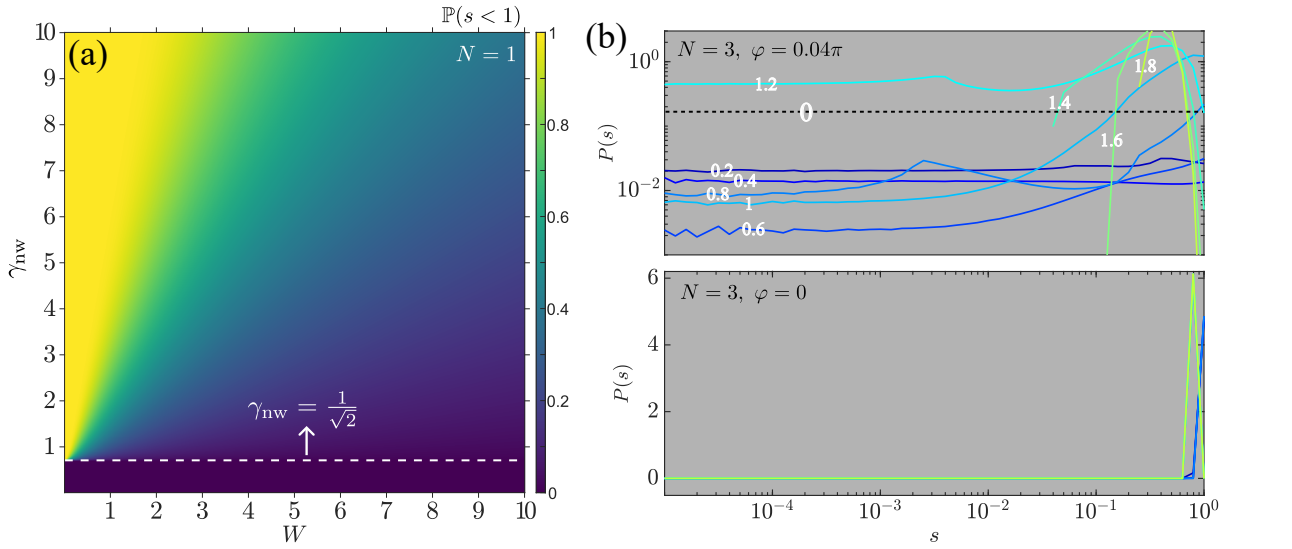

FIG. S7. Correlation statistics of the transmission output. (a) Probability of PA versus $\gamma_{\rm nw}$ and W. Here $N = 1$. (b) PDFs for different $\gamma_{\rm nw}$, with the values of $\gamma_{\rm nw}$ being indicated besides each curve. The chosen parameters are $\{N = 3, \varphi = 0.04\pi, W = 0.14\}$ (top) and $\{N = 3, \varphi = 0, W = 1\}$ (bottom), which are the same as Figs. 2(a,b) of the main text. These results are obtained from 10^{10} disorder realizations.

is defined as

$$\mathrm{H}(q(x), p(x)) = \frac{1}{2}\int \left(\sqrt{p(x)} - \sqrt{q(x)}\right)^2 \mathrm{d}x\,. \tag{S49}$$

The Hellinger distance measures the similarity between $p(x)$ and $q(x)$; its values range from 0 to 1, with values closer to 0 indicating that the two distributions are more similar. From Figs. S6(b-e), one can see that (i) the fidelity is close to 1 for both the single- and two-excitation steady states as the disorder strength increases, and (ii) the value of $\mathrm{H}(P(s), \tilde{P}(s))$ approaches 0 both for both the transmission and reflection outputs as the disorder strength increases. This implies that Eqs. (S46,S47) are indeed good approximations in the strong-disorder limit. Note that, although we only calculated the case of $N = 10$ here, similar results can be obtained for other chain sizes.

In Figs. S6(f-i), we present $P(10^{-3})$ and $\mathbb{P}(s < 1)$ versus different disorder strengths. For the transmission output, our results indicate that both $P(10^{-3})$ and $\mathbb{P}(s < 1)$ decrease as the disorder strength increases. This decrease follows a scaling of the form W^{-3}, regardless of the chain size. For the reflection output, the probability of NPPB increases with increasing disorder strength, while the probability of PA saturates to a constant in the limit $W \gg 1$. This constant is close to 2/3, i.e., the value of $\mathbb{P}(s < 1)$ for a system with $N = 2$ and $\varphi = 0$. This result is also consistent with Fig. 4(c) of the main text, where $\mathbb{P}(s < 1)$ is calculated based on Eq. (S18).

V. EFFECTS OF LOSSES ON NON-WAVEGUIDE MODES

In this section, we consider losses to modes external to the waveguide. With such losses, the non-Hermitian Hamiltonian becomes

$$H_{\rm eff} = \sum_{m,n=1}^{N} \left(\Delta_m \delta_{m,n} - \frac{i\gamma_{\rm nw}}{2}\delta_{m,n} - \frac{i\gamma}{2}e^{i|m-n|\varphi}\right)\sigma_m^\dagger \sigma_n, \tag{S50}$$

where $\gamma_{\rm nw}$ denotes the decay rate to non-waveguide modes. Again, we set $\gamma = 1$ in the remainder of this section and use the symbol β to represent the coupling efficiency. The definition of β is $\beta = \gamma/(\gamma + \gamma_{\rm nw}) = (1 + \gamma_{\rm nw})^{-1}$. In the main text, we set $\gamma_{\rm nw} = 0$, corresponding to a unit value of the coupling efficiency.

A. Transmission output

We first consider the single-qubit system, for which $\mathbb{P}(s<1)$ and $P(0)$ can be analytically calculated. In this case, the correlation function is given by

$$g_{\mathrm{T}}=\frac{(4\Delta_1^2+(\gamma_{\mathrm{nw}}-1)^2)(4\Delta_1^2+(\gamma_{\mathrm{nw}}+1)^2)}{(4\Delta_1^2+\gamma_{\mathrm{nw}}^2)^2}. \tag{S51}$$

Before proceeding to disordered systems, let us first focus on clean systems. For a resonant qubit, i.e., $\Delta_1=0$, the correlation function is $g_{\mathrm{T}}=(\gamma_{\mathrm{nw}}^2-1)^2/\gamma_{\mathrm{nw}}^4$, which satisfies $g_{\mathrm{T}}<1$ for $\gamma_{\mathrm{nw}}>1/\sqrt{2}$ ($\beta\lesssim 0.58$) and $g_{\mathrm{T}}=0$ for $\gamma_{\mathrm{nw}}=1$ ($\beta=1/2$). Unlike lossless system, here the transmission output can produce either antibunched or perfectly blockaded photons by appropriately adjusting the coupling efficiency.

Considering the effects of disorder, the probability of PA is calculated as

$$\begin{aligned}\mathbb{P}(s<1)&=\frac{1}{\sqrt{2\pi}W}\int_{-\infty}^{\infty}e^{-\Delta_1^2/2W^2}\Theta\left(\frac{(4\Delta_1^2+(\gamma_{\mathrm{nw}}-1)^2)(4\Delta_1^2+(\gamma_{\mathrm{nw}}+1)^2)}{(4\Delta_1^2+\gamma_{\mathrm{nw}}^2)^2}-1\right)\mathrm{d}\Delta_1\\&=\frac{1}{\sqrt{2\pi}W}\int_0^{\frac{\gamma_{\mathrm{nw}}^2}{4}-\frac{1}{8}}\frac{e^{-\Delta_1/2W^2}}{\sqrt{\Delta_1}}\Theta\left(\gamma_{\mathrm{nw}}-\frac{1}{\sqrt{2}}\right)\mathrm{d}\Delta_1\\&=\mathrm{erf}\left(\frac{\sqrt{\gamma_{\mathrm{nw}}^2/4-1/8}}{\sqrt{2}W}\right)\Theta\left(\gamma_{\mathrm{nw}}-\frac{1}{\sqrt{2}}\right),\end{aligned} \tag{S52}$$

where $\mathrm{erf}(x)$ is the error function. This result shows that when a single qubit is strongly coupled to the waveguide, PA in the transmission output is impossible. By reducing the coupling efficiency until reaching a critical value $\beta_{\mathrm{cri}}=1/(1+1/\sqrt{2})\approx 0.58$, PA events can be observed. For $\beta<\beta_{\mathrm{cri}}$, the probability of PA increases as the coupling efficiency decreases, as shown in Fig. S7(a).

As for $P(0)$, we first calculate the PDF. After performing the integral (similar to Eq. (S20)), the PDF for $s<1$ is given by

$$\begin{aligned}P(s)=-\frac{1}{\sqrt{2\pi}W}&\frac{(-1+\sqrt{s+4(1-s)\gamma_{\mathrm{nw}}^2})^3}{4\sqrt{-1+(s-1)\gamma_{\mathrm{nw}}^2+\sqrt{s+4(1-s)\gamma_{\mathrm{nw}}^2}}(s-1)^2(4(s-1)\gamma_{\mathrm{nw}}^2-s+\sqrt{s+4(1-s)\gamma_{\mathrm{nw}}^2})(1-s)^{3/2}}\times\\&\exp\left(\frac{-1+(s-1)\gamma_{\mathrm{nw}}^2+\sqrt{s+4(1-s)\gamma_{\mathrm{nw}}^2}}{(8s-8)W^2}\right),\end{aligned} \tag{S53}$$

where $\gamma_{\mathrm{nw}}>1/\sqrt{2}$ and $1+\gamma_{\mathrm{nw}}^{-4}-2\gamma_{\mathrm{nw}}^{-2}<s<1$. From this result, $P(0)=0$ for $\beta\neq 1/2$ ($\gamma_{\mathrm{nw}}\neq 1/2$); only when the coupling efficiency is exactly $1/2$, $P(s)$ diverges as $P(s)\sim(W\sqrt{s})^{-1}$, whereby PPB events become possible.

In Figs. S8(a,b), we present the numerical results for the probability of PA for $N=5$ and $N=10$. These results show that the probability of PA can be efficiently enhanced by decreasing the coupling efficiency (by increasing γ_{nw}). In particular, the probability of PA can reach unit provided that the chain is highly dense, i.e., $\varphi\ll 1$. We then calculate the PDFs for the system with $N=3$ [see Fig. S7](b). When $\varphi\neq 0$, the results show that as the coupling efficiency decreases, the PDFs still exhibit a constant behavior at $s\ll 1$ as long as $\beta\gtrsim 0.45$; this behavior disappears for $\beta\lesssim 0.45$. For $\beta\gtrsim 0.45$, the value of $P(s)$ at $s\ll 1$ can even be larger than that for lossless systems ($\gamma_{\mathrm{nw}}=0$). This is observed, for instance, when $\gamma_{\mathrm{nw}}=1.2$ ($\beta\approxeq 0.45$). Therefore, we still use $P(10^{-3})$ as a measure for the probability of NPPB and present the results for different system parameters in Figs. S8(c,d). The results show that the probability of NPPB attains a larger value when the coupling efficiency is not too high ($\beta\lesssim 0.5$). Moreover, when $\varphi=0$, the generation of strongly antibunched photon is impossible [see Fig. S7], similar to the system with $\beta=1$.

B. Reflection

In Figs. S9(a,b), we present the results of the probability of PA for $N=5$ and $N=10$. As the coupling efficiency decreases, a high probability of PA can only be achieved when the chain is highly dense, which is similar to the transmission output. Besides, it maintains a finite value even for strong disorder strength. This is because the effects of losses will be suppressed by strong disorder. We also investigate the behavior of $P(s_0)$ at $s_0\ll 1$ when $W\gg 1$. In

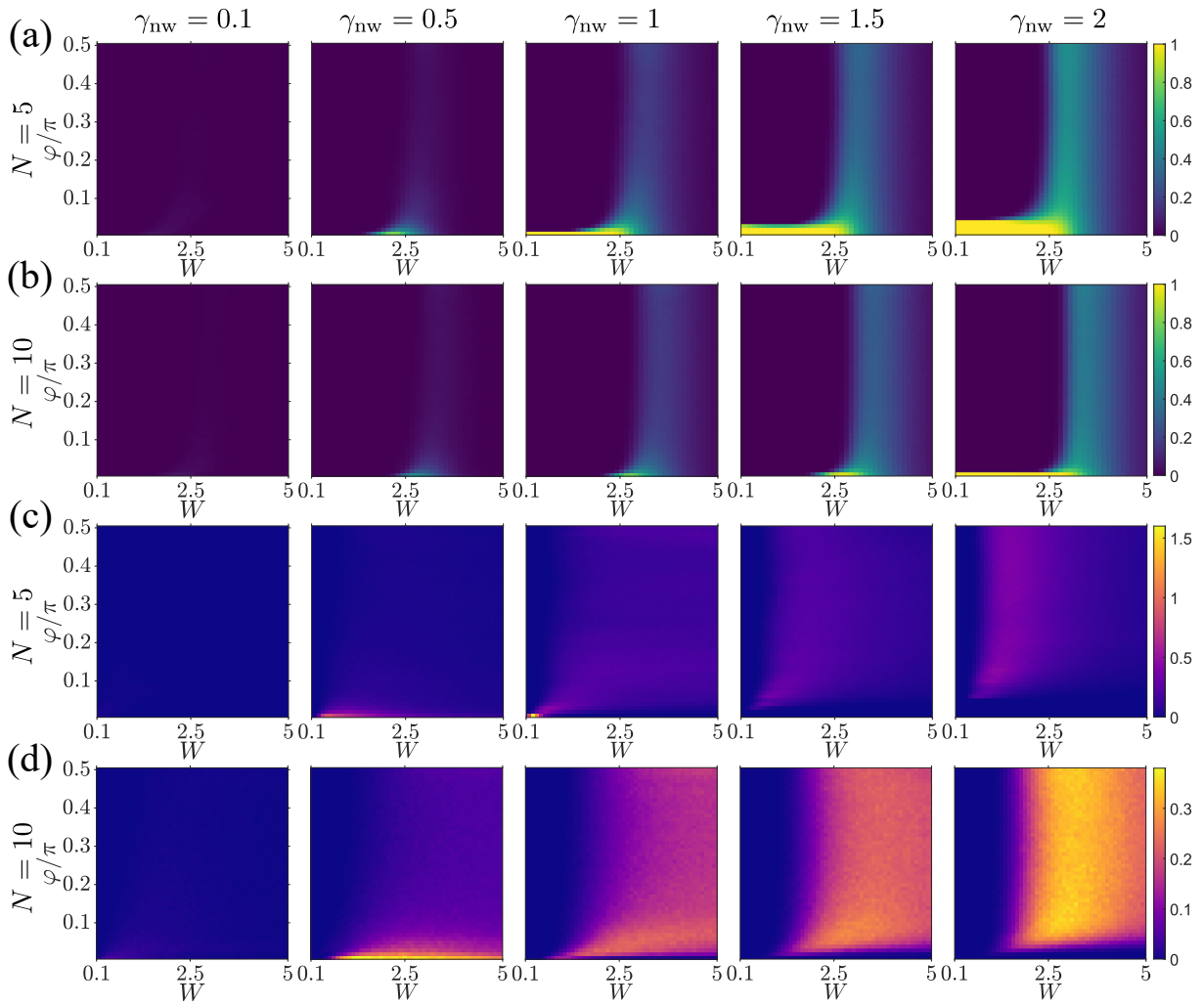

FIG. S8. Correlation statistics of the transmission output. (a,b) Probability of PA versus φ and W for different N and $\gamma_{\rm nw}$. (c,d) $P(10^{-3})$ versus φ and W for different N and $\gamma_{\rm nw}$. These results for $\mathbb{P}(s<1)$ ($P(10^{-3})$) are obtained from 5^4 (5×10^6) disorder realizations.

this limit, the correlation function is given by

$$g_{\rm R} = \frac{|P_{\rm R}^{\mathcal{II}}|^2}{|P_{\rm R}^{\mathcal{I}}|^4} = \frac{|2\sum_{m>n}\frac{e^{2i(m+n)\varphi}}{(\Delta_m - i/2 - i\gamma_{\rm nw}/2)(\Delta_n - i/2 - i\gamma_{\rm nw}/2)}|^2}{|\sum_m \frac{e^{2im\varphi}}{\Delta_m - i/2 - i\gamma_{\rm nw}/2}|^4}. \tag{S54}$$

The numerical results in Figs. S9(c,d) show clearly that the probability of NPPB increases with increasing disorder strength, which is similar to systems where $\beta = 1$.

VI. EFFECTS OF CHIRALITY IN COUPLING TO WAVEGUIDE MODES

In this section, we consider chirality in coupling to waveguide modes, i.e., $\gamma_{\rm T} \neq \gamma_{\rm R}$. We define the chirality as $\alpha = \gamma_{\rm R}/\gamma_{\rm T}$, and we set $\gamma_{\rm T} = 1$ as the energy unit. Figures S10(a1) show the photon correaltions for transmission output, for system with chain size $N = 10$. The chirality together with the losses on non-waveguide modes significantly affect photon correlations. For transmission output, when qubits weakly coupled to waveguide ($\beta \ll 1$), photons maintain the coherence for all values of chirality; while when qubits strongly coupled to waveguide ($\beta \approx 1$), photons exhibit strong bunching for $\alpha \gtrsim 0.5$, and antibunched even strongly antibunched photon emerge by further increasing chirality (decreasing α). When the qubits are weakly coupled to the waveguide in a perfectly chiral fashion, the transmitted photon exhibit Poisson statistics for small system size, $N = 10$. As the chain size increases, the output

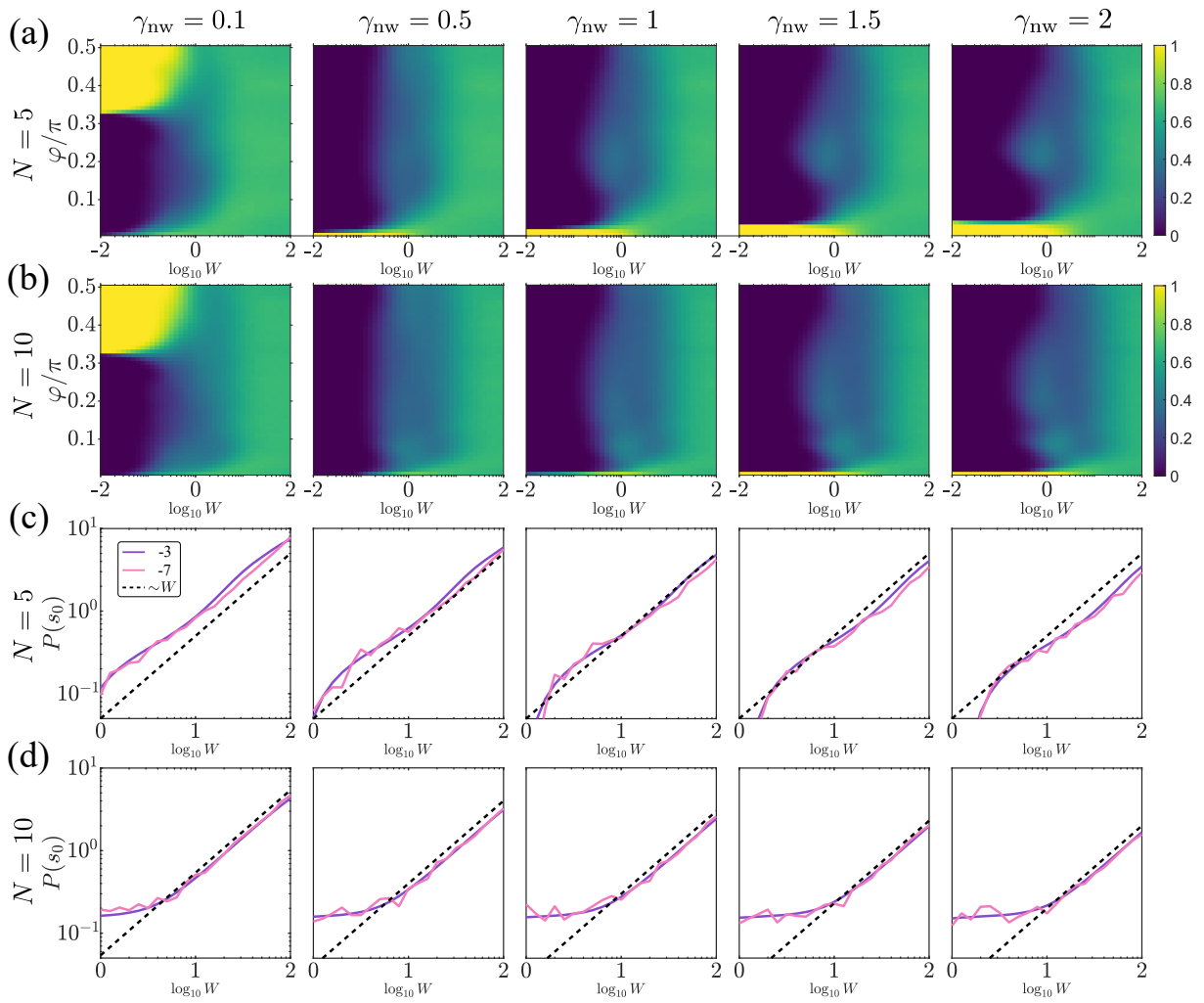

FIG. S9. Correlation statistics of the reflection output. (a,b) Probability of versus φ and W for different N and $\gamma_{\rm nw}$. (c,d) Solid lines denote $P(10^{\mu})$ versus φ and W for different N and $\gamma_{\rm nw}$, with the values of $\mu = -3,\ -7$. Dashed lines represent the numerical fits of $\sim W$. These results for $\mathbb{P}(s < 1)$ ($P(s_0)$) are obtained from 5^4 (5×10^{10}) disorder realizations.

becomes antibunched and approaches near-perfect antibunching at the optimal chain size $N \approx 183$; beyond this optimal chain size the output light becomes bunched as N increases further [see Fig. S10(a2)]. Note that these behaviors are quantitatively consistent with Fig. 3a in [10].

In the presence of disorder, Figs. S10(b1-c2) show $\mathbb{P}(s < 1)$ and $P(10^{-3})$ for the case of complete transimission-chirality ($\alpha = 0$). On the one hand, the probability of photon antibunching approach unit when qubits weakly coupled to waveguide, and rapidly decrease with increasing coupling strength. On the other hand, the probability of strong photon antibunching exhibits non-negligible value only for $0.1 \lesssim \beta \lesssim 0.4$. Notably, for the chain size investigated here $N = 10, 20$, these behaviors of $\mathbb{P}(s < 1)$ and $P(10^{-3})$ do not change significantly with changing N. Considering that when $N \sim 10^2$, the qubit number significantly affects the correlations even without the presence of disorder, we expect that $\mathbb{P}(s < 1)$ and $P(10^{-3})$ may show quite distinctive behaviors with further increasing N, in comparison with the results provided here.

VII. EFFECTS OF FINITE BANDWIDTH OF INPUT STATE

In this section, we consider the effects of finite bandwidth of the input state, which should be compared with the single-mode (zero bandwidth) coherent input state considered in the main text. We assume that the input state has

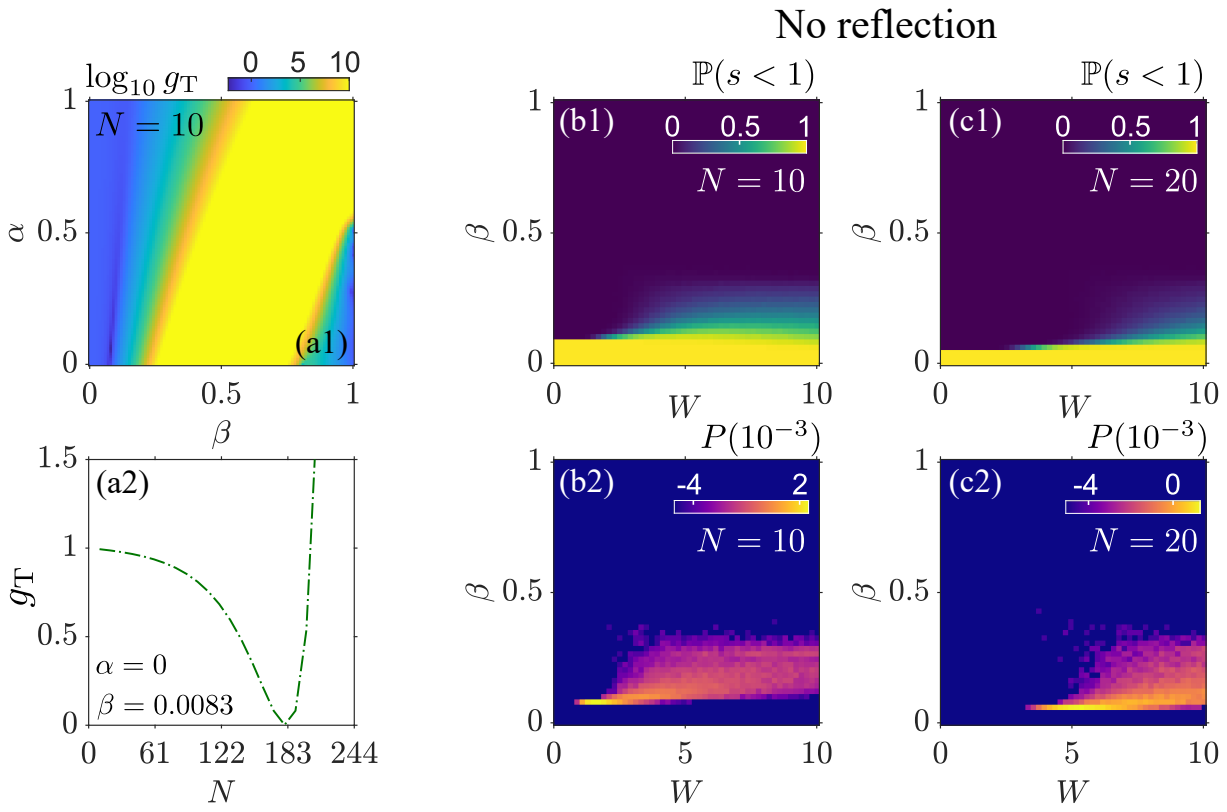

FIG. S10. (a1) Photon correlations in the transmission output versus chirality and coupling strength for $N = 10$ and $\varphi = 0$. (a2) Photon correlations in the transmission output versus chain size. Here the chosen parameters are $\alpha = 0$ and $\beta = 0.0083$. (b1,c1) Probability of photon antibunching in the transmission output versus disorder and coupling strength. $N = 10$ in (b1) and $N = 20$ in (c1). (b2,c2) $P(10^{-3})$ in the transmission output versus disorder and coupling strength. $N = 10$ in (b2) and $N = 20$ in (c2). $\alpha = 0$ in (b1-c2). Results are obtained from 10^5 disorder realizations.

the form

$$\rho_E(t_0) \propto \exp\left(\bar{n}\int_{-\infty}^{\infty}\alpha(\omega)a_T(\omega) - \alpha(\omega)a_T^\dagger(\omega)\,\mathrm{d}\omega\right). \tag{S55}$$

Here, $\alpha(\omega)$ controls the profile of the input state and is required to be normalized, i.e., $\int(\alpha(\omega))^2\,\mathrm{d}\omega = 1$, such that $\bar{n}^2 = \int_{-\infty}^{\infty}\mathrm{Tr}\left[\rho_E a_T^\dagger(\omega)a_T(\omega)\right]\mathrm{d}\omega$ represents the total number of photons in the input state, and we still consider the weak-input limit $\bar{n}^2 \ll 1$. To be able to compare with the case of zero bandwidth, we require $\alpha(\omega)$ to exhibit two following generic features: (i) $\alpha(\omega)$ approaches its maximum at ω_0 and rapidly decreases to zero for ω away from ω_0; (ii) a characteristic bandwidth denoted by σ_ω is able to characterize the width of $\alpha(\omega)$, such that $\sigma_\omega \to 0$ ($\sigma_\omega \to \infty$) corresponds to a ideal zero-bandwidth input (δ-pulse input in the time domain). Hereafter, we consider $\alpha(\omega)$ to be Lorentz profile, i.e., (we assume $\gamma = 1$)

$$\alpha(\omega) = \frac{1}{\mathcal{N}}\frac{\sigma_\omega}{(\omega-\omega_0)^2+\sigma_\omega^2}, \tag{S56}$$

where $\mathcal{N} = (\pi/2\sigma_\omega)^{1/2}$ denotes the normalization factor. The total number of photons in the time domain is given by

$$\bar{n}^2(t) = \int \mathrm{Tr}\Big\{a_T^\dagger(\omega,t)a_T(\omega,t)\rho_E(t_0)\Big\}\,\mathrm{d}\omega = \frac{1}{\sqrt{2\pi}}\int \mathrm{Tr}\Big\{e^{-i\omega(t-t_0)}a_T^\dagger(\omega)a_T(\omega)\rho_E(t_0)\Big\}\,\mathrm{d}\omega = \bar{n}^2\frac{e^{-\sigma_\omega|t-t_0|}(1+\sigma_\omega|t-t_0|)}{\sqrt{2\pi}}. \tag{S57}$$

This expression demonstrates that the input is also a wave package in the time domain, where $\bar{n}^2(t)$ approaches its maximum at $t = t_0$ and rapidly decreases for t away from t_0.

In this case, the master equation is still given by Eq. (S8), with

$$f(t-t_0, md) = \bar{n}\sqrt{\sigma_\omega}e^{-\sigma_\omega|t-t_0-md/v_g|}e^{-i\omega_0(t-t_0-md/v_g)} \approx \bar{n}\sqrt{\sigma_\omega}e^{-\sigma_\omega|t-t_0|}e^{-i\omega_0(t-t_0)}, \tag{S58}$$

where we assume that photons are injected far from the atomic ensemble, such that $t_0 + md/v_g \approx t_0$. Consequently, the correlation function can be obtained as

$$g_\mu(\tau,\tau) = \frac{\mathrm{Tr}\left[\rho(\tau)a^\dagger_{\mu,\mathrm{out}}(\tau)a^\dagger_{\mu,\mathrm{out}}(\tau)a_{\mu,\mathrm{out}}(\tau)a_{\mu,\mathrm{out}}(\tau)\right]}{\mathrm{Tr}\left[\rho(\tau)a^\dagger_{\mu,\mathrm{out}}(\tau)a_{\mu,\mathrm{out}}(\tau)\right]^2}, \tag{S59}$$

where $\rho(\tau)$ denotes the density matrix of atomic ensemble governed by the master equation. The input-output relations read as

$$a_{\mathrm{T,out}}(\tau) = a_{\mathrm{T,in}}(\tau) - i\sqrt{\frac{\gamma}{2}}\sum_m e^{-imd}\sigma_m(\tau), \quad a_{\mathrm{R,out}}(\tau) = -i\sqrt{\frac{\gamma}{2}}\sum_m e^{imd}\sigma_m(\tau), \tag{S60}$$

with

$$a_{\mathrm{T,in}}(\tau) = \frac{1}{\sqrt{2\pi}}\int \mathrm{Tr}\left[\rho_E(t_0)e^{-i\omega(\tau-t_0)}a_{\mathrm{T}}(\omega,t_0)\right]\mathrm{d}\omega = \bar{n}\sqrt{\sigma_\omega}e^{-\sigma_\omega|\tau-t_0|}e^{-i\omega_0(\tau-t_0)}. \tag{S61}$$

Before proceeding to present the results for the correlation functions, we stress that, in addition to the bandwidth σ_ω, the evolution time τ will also significantly affect the photon correlation. For a ideal zero-bandwidth input, the correlation functions g_μ are time-independent for $t \gg 1$, and thus their values can be obtained from the steady state of the atomic ensemble. This actually arises from the fact that the drive strength $\propto |f(t-t_0, md)|$ remains a constant in the time domain. However, for a finite-bandwidth input, the drive strength is now time-dependent, therefore, one should expect that $g_\mu(\tau,\tau)$ is also dependent on the evolution time τ.

In Fig. S11(a), we present the photon correlation in the transmission output for $N = 1$ with $\Delta_1 = 0$. For a ideal zero-bandwidth input, $g_T = \infty$. Our result reveals that $g_{\mathrm{T}}(\tau,\tau)$ generally recovers its zero-bandwidth counterpart when $\sigma_\omega \ll 1$. This is because, when the bandwidth is much smaller than the individual decay rate γ, the input can be approximately considered as a zero-bandwidth coherent state, resulting in $g_{\mathrm{T}}(\tau,\tau) \gg 1$. Increasing σ_ω, $g_{\mathrm{T}}(\tau,\tau)$ becomes sensitive to the evolution time τ: its value still approximately recovers the zero-bandwidth counterpart for $\tau \sim t_0$; while for $|\tau - t_0| \gg 1$, $g_{\mathrm{T}}(\tau,\tau)$ significantly deviates from infinity, which can even approaches near zero. In Figs. S11(b,c), we present the probability of PA for system with $N = 2$ and $\varphi = 0$, and the probability density functions for system with $N = 3$ and $\varphi = 0.5\pi$ in the reflection output. The obtained results show good agreement with their zero-bandwidth counterpart as long as $\sigma_\omega/\gamma \lesssim 0.1$, i.e., $\mathbb{P}(s<1) = 2/3$ and $P(s \ll 1) \neq 0$.

In summary, when one considers the effect of finite band width of input state, the obtained results show good agreement with their zero-bandwidth counterpart, as long as the bandwidth σ_ω is much smaller than the individual decay rate γ, and the detection time τ is appropriately chosen. In typical waveguide QED platforms, $\gamma \sim$ MHz, therefore, the required band width should be $\sigma_\omega \lesssim$ KHz, which can be achieved in the state-of-art waveguide platforms [7–9].

VIII. NUMERICAL CALCULATIONS OF $\mathbb{P}(s<1)$ AND $P(s \ll 1)$ FOR MANY-QUBIT SYSTEM

A. Calculation about $\mathbb{P}(s<1)$

The definition of $\mathbb{P}(s<1)$ is

$$\mathbb{P}(s<1) = \int_0^1 P(s)\mathrm{d}s = \int_{-\infty}^{\infty}\cdots\int_{-\infty}^{\infty}\Theta(g_\mu - 1)p(\Delta_1,\Delta_2,\cdots,\Delta_N)\mathrm{d}\Delta_1\cdots\mathrm{d}\Delta_N. \tag{S62}$$

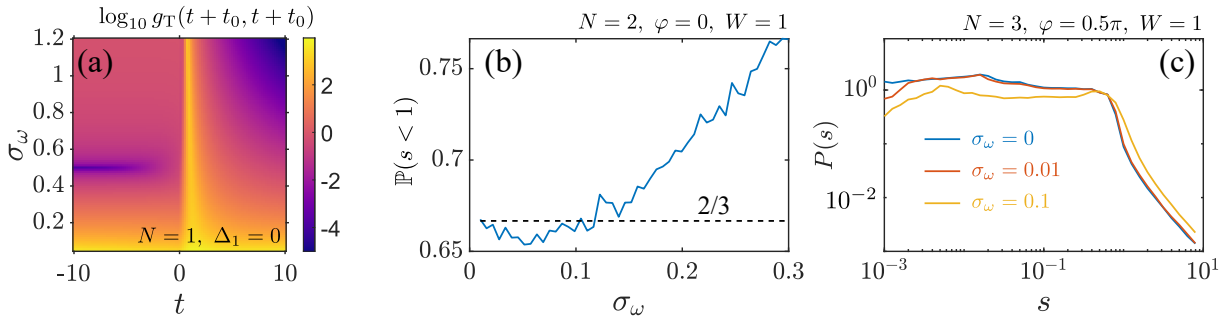

FIG. S11. (a) Photon correlation in the transmission versus bandwidth and evolution time for system with $N=1$ and $\Delta_1=0$. (b) Probability of photon antibunching in the reflection output versus band width for system with $N=2$ and $\varphi=0$. Results are obtained from 10000 disorder realizations. (c) Probability density function in the reflection output for different values of band width for system with $N=3$ and $\varphi=0.5\pi$. Results are obtained from 10^5 disorder realizations. $\tau=t_0$ in (b) and (c). $\bar{n}=0.1$ in (a-c).

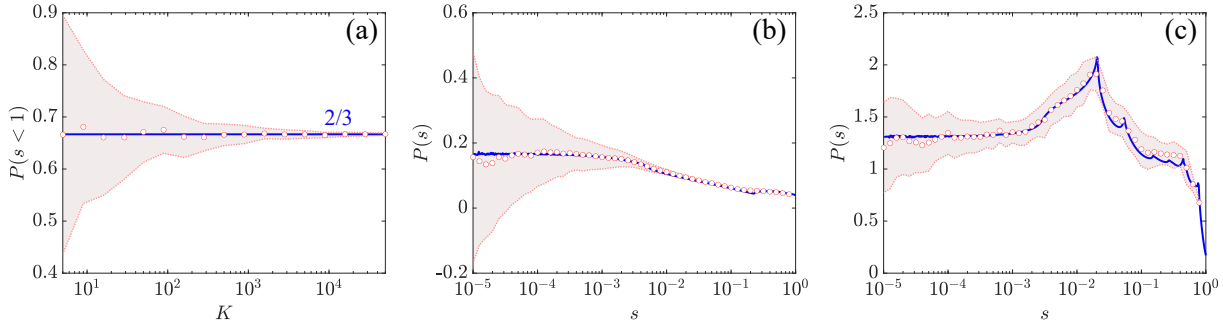

FIG. S12. (a) Probability of PA for the reflection output from the Monte Carlo integration. The result is obtained from 10^2 estimations. Red dots and the shaded area denote the mean value and the standard deviation of the estimations, respectively. Here the chosen parameter are $N=2$ and $\varphi=0$, so that the solid line represents the exact value of $\mathbb{P}(s<1)$, which is equal to 2/3. (b-c) PDFs for the transmission (b) and reflection (c) outputs from the Monte Carlo integration. The result is obtained from 10^2 estimations. Red dots and the shaded area denote the mean value and the standard deviation from Eq. (S64), respectively. The number of disorder realizations is $K=50000$. The solid blue lines represent the results from $K=10^{11}$ disorder realizations. Here the chosen parameters are $N=3$, $\varphi=0.04\pi$, and $W=0.15$ in (b); $N=3$, $\varphi=0.5\pi$, $W=1$ in (c).

According to the Monte Carlo method, this integral can be approximately evaluated by

$$\mathbb{P}(s<1)=E[\Theta(g_\mu-1)]\approx\frac{1}{K}\sum_{j=1}^{K}\Theta\Big(g_\mu\big|_{\vec{\Delta}_j}-1\Big), \tag{S63}$$

where $\vec{\Delta}_j=\{\Delta_{1,j},\cdots,\Delta_{N,j}\}$ denotes the j-th sample drawn from the i.i.d Gaussian distribution. The sample size K should be large enough to reduce the variance of the estimation in Eq. (S63), which is given by $V[\Theta(g_\mu-1)]\sim K^{-1}$. In Fig. S12(a), we present $E[\Theta(g_\mu-1)]$ for the reflection output versus the sample size K, with $N=2$ and $\varphi=0$. The mean and standard deviation are obtained from 10^2 estimations of Eq. (S63). As shown, $K\sim10^4$ is sufficient to reduce $V[\Theta(g_\mu-1)]$, so that the mean value deviate only slightly from the exact value of 2/3, even for a single estimation. Therefore, in the main text, we set $K=50000$ and perform a single estimation for all plots concerning $\mathbb{P}(s<1)$.

B. Calculation about $P(s \ll 1)$

Similarly, $P(s)$ can be approximately estimated by the Monte Carlo method according to

$$P(s) = E[\delta(g_\mu - s)] \approx \frac{1}{K}\sum_{j=1}^{K} \lim_{\varepsilon\to 0} \tilde{\delta}_\varepsilon\Big(g_\mu\big|_{\vec{\Delta}_j} - s\Big), \tag{S64}$$

where $\tilde{\delta}_\varepsilon(x)$ represents a function that weakly converges to the Dirac-delta function in the limit $\varepsilon \to 0$. Compare to the estimation in Eq. (S63), the estimation of $P(s)$, especially at $s \ll 1$, requires a larger number of disorder realizations to achieve an acceptable error. This is because the number of events $s - \epsilon < g_\mu < s + \epsilon$ with $\epsilon \ll s$ decreases with decreasing s. To see this, note that the probability of the event $s_0 - \epsilon < g_\mu < s_0 + \epsilon$, with $\epsilon \ll s_0$, is given by

$$\mathbb{P}(s_0 - \epsilon < s < s_0 + \epsilon) = \int_{s_0-\epsilon}^{s_0+\epsilon} P(s)\,\mathrm{d}s \sim P(s_0)\epsilon. \tag{S65}$$

Since we have shown that $P(s_0) \sim$ constant for $s_0 \ll 1$, this probability decreases as s_0 decreases, due to the condition $\epsilon \ll s_0$. In fact, the constant form of $P(s)$ implies that this probability scales as s; i.e., $\mathbb{P}(s_0 - \epsilon < s < s_0 + \epsilon) \sim s$ if we let $\epsilon = \eta s_0$ with $\eta \ll 1$. The decrease of $\mathbb{P}(s_0 - \epsilon < s < s_0 + \epsilon) \sim s$ means that the number of events with $s - \epsilon < g_\mu < s + \epsilon$ also decreases as s decreases. As a result, many estimations from Eq. (S64) for $s \ll 1$ will yield zero if K is not sufficiently large, because the value of $\tilde{\delta}_\epsilon(x)$ is proportional to the number of such events. Meanwhile, the computational cost increases rapidly with K, especially for large chain size. To balance the accuracy of the Monte Carlo integration results with the computational cost, an appropriate value of K must be chosen.

In Figs. S12(b,c), we compare the PDFs obtained from $K = 50000$ with those obtained from $K = 10^{11}$. For $K = 50000$, we perform 10^2 estimations so that the total sample size is 5^6. For $K = 10^{11}$, the variation in the estimation is negligible, and it can be regarded as the exact PDF. Compared to the estimation of Eq. (S63), the variation increases as s decreases s and becomes non-negligible for $s \ll 1$. However, despite the increased variation, the mean values from 10^2 are very close to the exact value. Therefore, unless otherwise noted, we set $K = 50000$ and perform 10^2 estimations using Eq. (S64) to obtain all plots related to $P(10^{-3})$ in the main text.

[1] T. Caneva, M. T. Manzoni, T. Shi, J. S. Douglas, J. I. Cirac, and D. E. Chang, "Quantum dynamics of propagating photons with strong interactions: a generalized input–output formalism," New Journal of Physics **17**, 113001 (2015).

[2] A. S. Sheremet, M. I. Petrov, I. V. Iorsh, A. V. Poshakinskiy, and A. N. Poddubny, "Waveguide quantum electrodynamics: Collective radiance and photon-photon correlations," Reviews of Modern Physics **95**, 015002 (2023).

[3] A. Asenjo-Garcia, M. Moreno-Cardoner, A. Albrecht, H. J. Kimble, and D. E. Chang, "Exponential Improvement in Photon Storage Fidelities Using Subradiance and "Selective Radiance" in Atomic Arrays," Physical Review X **7**, 031024 (2017).

[4] Y. Wang, W. Verstraelen, B. Zhang, T. C. H. Liew, and Y. D. Chong, "Giant Enhancement of Unconventional Photon Blockade in a Dimer Chain," Phys. Rev. Lett. **127**, 240402 (2021).

[5] T. C. H. Liew and V. Savona, "Single Photons from Coupled Quantum Modes," Phys. Rev. Lett. **104**, 183601 (2010).

[6] H. Flayac and V. Savona, "Unconventional photon blockade," Phys. Rev. A **96**, 053810 (2017).

[7] S. Faez, P. Türschmann, H. R. Haakh, S. Götzinger, and V. Sandoghdar, "Coherent interaction of light and single molecules in a dielectric nanoguide," Physical review letters **113**, 213601 (2014).

[8] B. Kuyken, T. Ideguchi, S. Holzner, M. Yan, T. W. Hänsch, J. Van Campenhout, P. Verheyen, S. Coen, F. Leo, R. Baets, *et al.*, "An octave-spanning mid-infrared frequency comb generated in a silicon nanophotonic wire waveguide," Nature communications **6**, 6310 (2015).

[9] Z. Bao, Y. Li, Z. Wang, J. Wang, J. Yang, H. Xiong, Y. Song, Y. Wu, H. Zhang, and L. Duan, "A cryogenic on-chip microwave pulse generator for large-scale superconducting quantum computing," Nature Communications **15**, 5958 (2024).

[10] A. S. Prasad, J. Hinney, S. Mahmoodian, K. Hammerer, S. Rind, P. Schneeweiss, A. S. Sørensen, J. Volz, and A. Rauschenbeutel, "Correlating photons using the collective nonlinear response of atoms weakly coupled to an optical mode," Nature Photonics **14**, 719 (2020).